Nucleic Acids Research, 2021 **1**
https://doi.org/10.1093/nar/gkab993

HI-NESS: a family of genetically encoded DNA labels based on a bacterial nucleoid-associated protein

Fatema-Zahra M. Rashid[1,2], Eike Mahlandt[3], Michiel van der Vaart[4], Daphne E.C. Boer[5], Monica Varela Alvarez[4], Bram Henneman[1], Daan J.W. Brocken[1], Patrick Voskamp[6], Anneloes J. Blok[1], Thomas S. Shimizu[7], Annemarie H. Meijer[4], Martijn S. Luijsterburg[5], Joachim Goedhart[3], Frédéric G.E. Crémazy[1] and Remus T. Dame[1,2,*]

[1]Macromolecular Biochemistry, Leiden Institute of Chemistry, Leiden University, Leiden 2333CC, The Netherlands, [2]Centre for Microbial Cell Biology, Leiden University, Leiden, The Netherlands, [3]Molecular Cytology, Swammerdam Institute for Life Sciences, University of Amsterdam, Amsterdam 1098XH, The Netherlands, [4]Animal Sciences, Institute of Biology Leiden, Leiden University, Leiden 2333CC, The Netherlands, [5]Department of Human Genetics, Leiden University Medical Center, Leiden 2333ZC, The Netherlands, [6]Biophysical Structural Chemistry, Leiden Institute of Chemistry, Leiden University, Leiden 2333CC, The Netherlands and [7]Systems Biology, AMOLF Institute, Amsterdam 1098XG, The Netherlands

Received November 03, 2020; Revised October 06, 2021; Editorial Decision October 07, 2021; Accepted October 08, 2021

ABSTRACT

The interplay between three-dimensional chromosome organisation and genomic processes such as replication and transcription necessitates *in vivo* studies of chromosome dynamics. Fluorescent organic dyes are often used for chromosome labelling *in vivo*. The mode of binding of these dyes to DNA cause its distortion, elongation, and partial unwinding. The structural changes induce DNA damage and interfere with the binding dynamics of chromatin-associated proteins, consequently perturbing gene expression, genome replication, and cell cycle progression. We have developed a minimally-perturbing, genetically encoded fluorescent DNA label consisting of a (photo-switchable) fluorescent protein fused to the DNA-binding domain of H-NS — a bacterial nucleoid-associated protein. We show that this DNA label, abbreviated as HI-NESS (H-NS-based indicator for nucleic acid stainings), is minimally-perturbing to genomic processes and labels chromosomes in eukaryotic cells in culture, and in zebrafish embryos with preferential binding to AT-rich chromatin.

INTRODUCTION

Developments in the field of chromosome biology have highlighted an intricate interplay between the spatiotemporal organisation of the chromosome and its activities such as transcription, replication, and segregation (1–3). Investigations of such time-resolved structural dynamics of chromosomes in live cells can be performed by fluorescence microscopy. Fluorescent organic dyes are often the first choice for labelling chromosomes. Bisbenzimides such as 6-diamidino-2-phenylindole (DAPI) and Hoechst insert into the minor groove of AT-rich double-stranded DNA (dsDNA), resulting in an enhanced fluorescence emission in the blue range of the visible spectrum (4–6). Hoechst 33258 has also been conjugated to other fluorescent dyes including, but not limited to, IR-786, fluorescein, and silicon-rhodamine (SiR), that shift its spectral properties from the phototoxic UV/blue range towards longer wavelengths of the spectrum (7–11). Cyanine dyes such as those of the TOTO, TO-PRO and SYTOX families intercalate between DNA bases and exhibit fluorescence emission enhancement (12–14). The amplified fluorescence of organic dyes upon DNA binding allows DNA labelling with a high signal-to-noise ratio. Due to the reversible binding of the fluorophores to DNA, this feature also allows the detection of single binding events that enables super-resolution imaging by binding-activated localization microscopy (BALM) and fluctuation-assisted BALM (15,16), and point accumulation for imaging in nanoscale topography (PAINT) (17,18). Stochastic blinking of fluorophores such as silicon-rhodamine and carboxyrhodamine conjugated to Hoechst allows super-resolution imaging with stimulated emission detection (STED) microscopy (10,11). Furthermore, bisbenzimides undergo stochastic photoconversion upon UV exposure that shifts the excitation and emission spectra of the dyes from the UV/blue to the blue/green and green/red ranges (19–21). While being problematic for multicolour

*To whom correspondence should be addressed. Tel: +31 71 527 5605; Email: rtdame@chem.leidenuniv.nl
Present address: Frédéric G.E. Crémazy, Laboratoire Infection et Inflammation, INSERM, UVSQ, Université Paris-Saclay, Versailles 78180, France.

fluorescence microscopy studies, this property is exploited in single molecule localisation microscopy (SMLM) to image chromatin in intact cell nuclei at a resolution of up to ∼40 nm (22,23).

Despite their broad use, the binding mode of organic DNA labels results in distortion, elongation, and/or partial unwinding of the double-helix (24–27). The structural changes interfere with the binding of DNA-processing enzymes and affect their enzymatic activity (28–32). Fluorescent organic dyes can also generate single- and double-strand breaks in the DNA owing to reactive oxygen species that are produced when the excited fluorophore reacts with molecular oxygen (33,34). DNA intercalation may also trigger DNA damage signalling and cell cycle arrest in the absence of laser excitation (35). Thus, fluorescent organic DNA dyes are generally cytotoxic, especially during prolonged incubation periods necessary for time-lapse experiments (35–38). Moreover, some fluorescent organic DNA dyes are unable to permeate the membrane of live cells, requiring cell fixation and the use of permeabilisation agents such as SDS and Triton X-100 for DNA staining. The dyes may strongly bind to RNA as well, calling for RNase A treatment prior to imaging (39).

An alternative approach that relies on covalent labelling of DNA with organic fluorophores has also been introduced. Covalent binding of azide-functionalized fluorophores such as tetramethylrhodamine azide (TAMRA) and Alexa Fluor-azide to alkyne-functionalized nucleotide analogues—EdU (5-ethynyl-2-deoxyuridine) and EdC (5-ethynyl-2-deoxycytidine) — with click chemistry (40) has been used to localize DNA in mammalian cells (41–43), plant tissues (44), and *Escherichia coli* (45–47). While affording resolutions of <20 nm with super-resolution microscopy techniques (41,45), this approach is of limited applicability in live cell imaging. The incorporation of EdU and EdC into DNA for prolonged periods (2 to 8 hours) triggers DNA damage signalling, interferes with cell cycle progression, and induces apoptosis (48,49). Fluorescent labelling of the nucleotide analogues requires cell fixation and permeabilisation, and Cu^{+} to catalyse the click reaction (40–47). Moreover, the covalent attachment of large fluorophores to chromosomal DNA would predictably be cytotoxic.

Chromosomes can also be visualised by the expression of fluorescent proteins fused to DNA-binding proteins. For eukaryotic systems, the histones H2B, H3 and H4 tagged with (photoactivatable) fluorescent proteins have been shown to incorporate into functional nucleosomes during the S-phase, and to accurately describe chromosome structure throughout the cell cycle (50–52). Such fusions have been used to obtain constitutive DNA staining in mice, nematodes, zebrafish, drosophila and arabidopsis transgenic strains (53–57). mEos2- and mEos3-tagged Heterochromatin protein 1 (HP1) have been used to study the distribution of heterochromatin in human embryonic stem cells at super-resolution (58). In bacterial systems, the distributions of fluorescently labelled nucleoid-associated proteins (NAPs) such as GFP-labelled α and β subunits of *Escherichia coli* HU (HupA and HupB, respectively) (59) and Fis (60), and GFP/mCherry-labelled HBsu (61,62), — the *Bacillus subtilis* homologue of HU—have been shown to overlap with that of DAPI indicating that such protein fusions may be used as alternative DNA labels. Indeed, HupA-mCherry, and GFP-Fis have been used to follow the structural changes to the *E. coli* nucleoid during growth and cell division (63,64), HupB-EGFP was used to stain the chromosome in *Mycobacterium smegmatis* to study the distribution of fluorescently-labelled Lsr2 and $Lsr2_{\Delta NTD}$ in single cells (65), and GFP-HBsu has been used to image the nucleoid in *Bacillus subtilis* using 3D-structured illumination microscopy (3D-SIM) to visualize high-density regions in the chromosome (66). However, fluorescent protein fusions to native cell proteins can impair protein function by interfering with protein folding and the equilibria of the protein's interactions with other macromolecules (61,67–69). Fluorescent protein fusions also require titration of expression levels to match that of the native protein. Furthermore, certain fusions have a limited applicability, for instance, fluorescently labelled histone proteins can only be used to visualise the chromosome in eukaryotic cells.

Collectively, this creates a need for a universal, minimally perturbing DNA label for visualizing chromosomes in live cells. To that end, we have designed a fusion protein that exploits the spectral properties of (photoactivatable) fluorescent proteins, and the DNA-binding properties of H-NS — a bacterial nucleoid-associated protein. We show that the DNA label, termed HI-NESS (H-NS-based indicator for nucleic acid stainings), is minimally perturbing to cells and does not trigger DNA damage signalling or interfere with cell cycle progression, accurately describes chromosome structure in eukaryotic cells in culture and live zebrafish, and is customizable with regards to the fluorescent protein used for its visualization.

MATERIALS AND METHODS

Cloning HI-NESS expression vectors

The HI-NESS constructs were assembled and cloned into pBAD33, pTEC19, pcDNA3.1(+) and pcDNA™5/FRT/TO vectors in a single step using Gibson Assembly (70). The constructs were verified by Sanger sequencing and archived as DH5α glycerol stocks. A complete list of the template plasmids used for Gibson Assembly and the HI-NESS vectors assembled therefrom is provided in Table 1. The plasmids designed in this study are deposited on Addgene.org.

HI-NESS imaging in *Escherichia coli*

E. coli cells (MG1655 and MG1655 Δ*hns*) were grown at 37°C in M9 medium (42 mM Na_2HPO_4, 22 mM KH_2PO_4, 19 mM NH_4Cl, 2.0 mM $MgSO_4$, 0.1 mM $CaCl_2$, 170 mM NaCl, 1× trace elements, 1% Bacto™ casamino acids (BD), 10 μg/ml thiamine (Sigma-Aldrich), 0.4% glycerol (PanReac Applichem)) with the appropriate antibiotics (Table 1). Trace elements were prepared as a 100× stock solution of the following composition per 100 ml: 0.1 g $FeSO_4{\cdot}7H_2O$, 0.6 g $CaCl_2{\cdot}2H_2O$, 0.12 g $MnCl_2{\cdot}4H_2O$, 0.08 g $CoCl_2{\cdot}6H_2O$, 0.07 g $ZnSO_4{\cdot}7H_2O$, 0.03 g $CuCl_2{\cdot}2H_2O$, 2 mg H_3BO_3 and 0.5 g EDTA·Na_2. The medium was supplemented with 0.1% (w/v) arabinose (Sigma-Aldrich) to

Table 1. List of plasmids used in this study

Plasmid	Plasmid backbone	Insert	Resistance marker	Reference
pBAD33	pBAD33	N/A	Chloramphenicol	(93)
pcDNA3.1(+)	pcDNA3.1(+)	N/A	Ampicillin; Neomycin	Invitrogen
pTEC19	pFPV27	E2-Crimson	Hygromycin	Addgene #30178 (94)
pmTurquoise2-C1	pEGFP-C1	mTurquoise2	Kanamycin; Neomycin	Addgene #60560 (83)
mEos3.2-C1	mEos3.2-C1	mEos3.2	Kanamycin; Neomycin	Addgene #54550 (85)
pLau53	pBAD24	eYFP	Ampicillin	(95)
pmScarlet-i_C1	pC1	mScarlet-I	Kanamycin	From TWJG Addgene #85044 (86)
LifeAct-mNeonGreen	pEGFP-N1	mNeonGreen	Kanamycin	From TWJG Addgene #98877 (96)
pmTurquoise2-H2A	pmTurquoise2-C1	H2A	Kanamycin	Addgene #36207 (83)
pRD128[B]	pBAD33	mTurquoise2_H-NSdbd	Chloramphenicol	This paper Addgene #163097
pRD129[B]	pBAD33	mEos3.2_H-NSdbd	Chloramphenicol	This paper Addgene #163098
pRD188[ET]	pcDNA3.1(+)	NLS_mEos3.2_H-NSdbd_NLS	Ampicillin; Neomycin	This paper Addgene #163099
pRD190	pcDNA3.1(+)	NLS_mEos3.2_NLS	Ampicillin; Neomycin	This paper Addgene #163100
pRD198[‡, B]	pBAD33	mEGFP_H-NSdbd	Chloramphenicol	This paper Addgene #163101
pRD393[B]	pFPV27	mEos3.2-H-NSdbd	Hygromycin	This paper Addgene #168774
pRD395[‡, B]	pBAD33	mCherry_H-NSdbd	Chloramphenicol	This paper Addgene #163102
pRD396[B]	pBAD33	eYFP_H-NSdbd	Chloramphenicol	This paper Addgene #163103
pRD397[ET]	pcDNA3.1(+)	NLS_mTurquoise2_H-NSdbd_NLS	Ampicillin; Neomycin	This paper Addgene #163104
pRD398[‡, ET]	pcDNA3.1(+)	NLS_mCherry_H-NSdbd_NLS	Ampicillin; Neomycin	This paper Addgene #163105
pRD399[‡, ET]	pcDNA3.1(+)	NLS_mEGFP_H-NSdbd_NLS	Ampicillin; Neomycin	This paper Addgene #163106
pRD400[ET]	pcDNA3.1(+)	NLS_eYFP_H-NSdbd_NLS	Ampicillin; Neomycin	This paper Addgene #163107
pRD403[B]	pBAD33	mScarlet-I_H-NSdbd	Chloramphenicol	This paper Addgene #163108
pRD404[B]	pBAD33	mNeonGreen_H-NSdbd	Chloramphenicol	This paper Addgene #163109
pRD405[ET]	pcDNA3.1(+)	NLS_mScarlet-I_H-NSdbd_NLS	Ampicillin; Neomycin	This paper Addgene #163110
pRD406[ET]	pcDNA3.1(+)	NLS_mNeonGreen_H-NSdbd_NLS	Ampicillin; Neomycin	This paper Addgene #163111
pRD421	pET28a	His-tag_TEV-cleavable linker_mEos3.2_H-NSdbd	Kanamycin	This paper Addgene #163112
pRD437[ES]	pcDNA™5/FRT/TO	NLS-mEos3.2-H-NSdbd-NLS	Ampicillin; Puromycin	This paper Addgene #168463
pRD438	pcDNA™5/FRT/TO	NLS-mEos3.2-NLS	Ampicillin; Puromycin	This paper Addgene #168464
pRD439[ES]	pcDNA™5/FRT/TO	NLS-mTurquoise2-H-NSdbd-NLS	Ampicillin; Puromycin	This paper Addgene #168465
pRD440[ES]	pcDNA™5/FRT/TO	NLS-mCherry-H-NSdbd-NLS	Ampicillin; Puromycin	This paper Addgene #168466
pRD441[ES]	pcDNA™5/FRT/TO	NLS-mEGFP-H-NSdbd-NLS	Ampicillin; Puromycin	This paper Addgene #168467
pRD442[ES]	pcDNA™5/FRT/TO	NLS-eYFP-H-NSdbd-NLS	Ampicillin; Puromycin	This paper Addgene #168468
pRD443[ES]	pcDNA™5/FRT/TO	NLS-mScarlet-I-H-NSdbd-NLS	Ampicillin; Puromycin	This paper Addgene #168469
pRD444[ES]	pcDNA™5/FRT/TO	NLS-mNeonGreen-H-NSdbd-NLS	Ampicillin; Puromycin	This paper Addgene #168470
pRD445	pFPV27	mEos3.2	Hygromycin	This paper Addgene #168775

[‡]Sequences for mCherry, and mEGFP were prepared with PCR and Gibson assembly.
[B]Plasmids for expressing HI-NESS in bacteria.
[ET]Plasmids for transiently expressing HI-NESS in eukaryotic cells.
[ES]Plasmids for preparing eukaryotic cell lines that stably express HI-NESS.

induce expression from the pBAD33 vector. For experiments that required DAPI labelling, the dye (DAPI, Sigma-Aldrich) was added to a final concentration of 10 μg/ml to cultures at an OD_{600} of ∼0.1. The cells were harvested at an OD_{600} of 0.2 by centrifugation at 3000 × g for 5 min and resuspended in M9 medium to an OD_{600} of ∼2.0. 4.0 μl of the culture was pipetted onto a 1 mm-thick, 1.5% agarose pad prepared on a microscope slide. A cover-slip was placed over the cells and the slide was sealed with nail polish. *E. coli* cells were visualised using a Leica TCS SPE or SP8 confocal microscope with a 64× oil immersion objective (NA 1.4) and excited by 405, 488 or 532 nm laser lines.

HI-NESS imaging in *Mycobacterium marinum*

Mycobacterium marinum expressing HI-NESS or the mEos3.2 fluorophore lacking the H-NS DNA binding domain were statically grown in 7H9 broth supplemented with ADC and 50 μg/ml hygromycin at 28°C. *M. marinum* cells in the logarithmic phase were collected by centrifugation 4000 × g for 10 min. The cells were resuspended in sterile PBS and stained with 10 μg/ml DAPI before imaging. Images were collected on a TCS SP8 (Leica) using a 40× oil-immersion objective (NA 1.30).

HI-NESS imaging in eukaryotic cell lines: cell culture and sample preparation

HeLa (CCL-2, American Tissue Culture Collection; Manassas, VA, USA) and U2OS (HTB-96, American Tissue Culture Collection, Manassas, VA, USA) cells were cultured in Dulbecco's modified Eagle's medium + GlutaMAX™-I (Giboc) with 10% fetal calf serum (Giboc) (DMEM + FCS) at 37°C in 7% CO_2. For transfection, 25 000–50 000 cells were seeded on 24 mm øcover-slips (Menzel, Thermo Fisher Scientific) in a six-well plate with 2 ml DMEM + FCS and cultured for 24 h. A transfection mix containing 0.5–1 μg plasmid (Table 1), linear polyethylenimine (PEI, pH 7.3, Polysciences) with a concentration of 1 mg/ml per 100 ng DNA, and 200 μl OptiMEM (Thermo Fisher Scientific) was added to each well. 24 h after transfection, cells were incubated with 2 mM thymidine (CAS: 50-89-5, Sigma-Aldrich) in DMEM + FCS for 18 h to increase the percentage of dividing cells. Thereafter, cells were washed twice with DMEM and incubated for another 5 h before imaging. For SiR-Hoechst labelling, the cells were incubated with 500 nM SiR-DNA (SC007, SpiroChrome Probes for Bioimaging) in DMEM, 4 h prior to imaging. HeLa and U2OS cells were imaged between 24 and 48 h after transfection in an Attofluor cell chamber (Thermo Fischer Scientific) in 1 ml of Microscopy medium (20 mM HEPES (pH 7.4),137 mM NaCl, 5.4 mM KCl, 1.8 mM $CaCl_2$, 0.8 mM $MgCl_2$ and 20 mM glucose) at 37°C.

Blood outgrowth endothelial cells (BOEC) were cultivated from healthy adult donor blood as described previously (71) and cultured in Endothelial Cell Growth Medium-2 BulletKit (CC-3162, Lonza) with 100 U/ml Penicillin (Thermo Fisher Scientific) and 100 μg/ml Streptomycin (Thermo Fisher Scientific), and 20% fetal calf serum (Giboc) (EGM+) at 37°C in 5% CO_2. Culture dishes and cover-slips were coated with 0.1% gelatin (CAS 9000-70-8, Merck) in phosphate-buffered saline 30 min prior to cell seeding. Transfection was performed with 2 μg endotoxin free plasmid, using the Neon™ Electroporation Transfection system (MPK5000, Invitrogen) with the associated Neon™ Transfection System 100 μl Kit (MPK10096, Invitrogen) generating a single pulse of 1300 V for 30 ms. Cells were seeded on 24 mm øcover-slips in a six-well plate with 2 ml EGM+ . BOECs were imaged between 24 and 48 h after microporation in an Attofluor cell chamber (Thermo Fischer Scientific) in 1 ml EGM+ at 37°C and 5% CO_2.

HI-NESS imaging in eukaryotic cell lines: spinning disk microscopy

Cells were imaged with a Nikon Ti-E microscope equipped with a Yokogawa CSU X-1 spinning disk unit, a 60× objective (Plan Apo, VC, oil, DIC, NA 1.4), a 100× objective (Apo, TIRF, oil, DIC, N2), Perfect Focus System, and the Nikon NIS elements software. Images were acquired with an Andor iXon 897 CCD camera. mTurquoise2 was imaged using a 440 nm laser line, a triple dichroic mirror (suitable for 440, 514, 561 nm laser) and a 460–500 nm emission filter. mEos3.2 was imaged using a 488 nm laser line, a triple dichroic mirror (suitable for 405, 488, 561 nm laser) and a 500 nm long pass emission filter. mEos3.2 was photoconverted with a 405 nm laser line and imaged using 561 nm laser line, a triple dichroic mirror (suitable for 405, 488, 561 nm laser) and a 600–660 nm emission filter.

HI-NESS imaging in eukaryotic cell lines: wide-field microscopy

Dividing cells were imaged on a Nikon Ti-E widefield microscope, equipped with a 60x objective (Plan Apo λ, 60×, oil) and a 20× air objective (Plan Apo, VC, DIC, N2), a Lumencor Spectra X light source, the Perfect Focus System, a Hamamatsu C11440-22C camera (SN:100256), and Nikon NIS elements software. For overnight time lapse movies, HeLa cells were imaged in DMEM + FCS at 37°C and 5% CO_2 in an Attofluor cell chamber (Thermo Fischer Scientific) in a humidified environment. mTurquoise2 was imaged with an excitation wavelength of 440/20 nm and emission light was detected at 459–499 nm with an emission filter in combination with a dichroic mirror (455–491, 523–557, 590–800 nm transmission bands). mScarlet-I was imaged with an excitation wavelength of 550/15 nm and emission light was detected at 570–616 nm with an emission filter in combination with a dichroic mirror (411–452, 485–541, 567–621, 656–793 nm transmission bands). Phase contrast images were acquired with the phase contrast condenser PH3.

HI-NESS imaging in eukaryotic cell lines: confocal microscopy

Confocal microscopy images were obtained at a Leica SP8 equipped with a 63x objective (HC PL Apo, C2S, NA 1.40, oil), the pinhole was set to 1 Airy unit, using line scan, 4× frame averaging, at a scan speed of 40 Hz. SiR-Hoechst was imaged using a 633 nm laser line, emission light was detected between 642 and 788 nm with a HyD detector and

Table 2. List of antibodies used in this study

	Antibody	Dilution	Binding	Company (reference)
1st	γH2AX	WB and IF 1:1000	Human anti mouse	Millipore, #05-636 (JBW301)
	GFP	WB 1:1000	Human anti rabbit	Abcam, #ab290
2nd	Mouse IgG (H + L) CF770	WB 1:10 000	Goat anti mouse	Biotium, VWR #20077
	Rabbit IgG (H + L) CF680	WB 1:10 000	Goat anti rabbit	Biotium, VWR #20067
	Anti-Mouse Alexa 647	IF 1:1000	Goat anti mouse	Thermo fisher Scientific, #A21235

the gain was set to 50 V. mTq2 was imaged using a 442 nm laser line, emission light was detected between 452–598 nm with a HyD detector and the gain was set to 40 V. mEos3.2 was imaged using a 488 nm laser line, emission light was detected between 495–554 nm with a HyD detector and the gain was set to 110 V.

Line scan analysis

Line scans were performed using the 'Plot profile' function in Fiji (72). All profiles were normalized to the most intense pixel of the line scan that was assigned an arbitrary intensity value of 1000.

Cell lines

U2OS Flp-In/T-REx (U2OS (FRT)) cells (73) were co-transfected with 5 μg of pRD441 (Table 1) and 0.5 μg of pOG44 encoding the Flp recombinase (Invitrogen™) using lipofectamine 2000 (Invitrogen™). U2OS (FRT)-NLS-mEGFP-HNSdbd-NLS (U2OS (FRT)-HI-NESS) cells were selected by incubation with 1 μg/ml puromycin and subsequently used to stably express mEGFP-tagged HI-NESS by the addition of 2 μg/ml doxycycline for 24 h.

U2OS (FRT) (73), U2OS (FRT)-mEGFP-NLS (74), and U2OS (FRT)-HI-NESS were cultured at 37°C and 5% CO_2 in DMEM (Thermo Fisher Scientific) supplemented with penicillin/streptomycin (Sigma) and 10% fetal bovine serum (FBS; Bodinco BV). U2OS (FRT) cells, which were generated using the Flp-In™/T-REx™ system (Thermo Fisher Scientific), were a gift from Daniel Durocher.

Western blotting

Proteins were separated on 4–12% Criterion XT Bis–Tris gels (Bio-Rad, #3450124) in NuPAGE MOPS running buffer (NP0001-02 Thermo Fisher Scientific), and blotted onto PVDF membranes (IPFL00010, EMD Millipore). Membranes were blocked with blocking buffer (Rockland, MB-070-003) for 1 h at 25°C. Membranes were then probed with antibodies (Table 2) as indicated. Proteins were detected using the Odyssey CLx Imaging System (LI-COR).

EdU labelling

Cells were seeded on 12 mm coverslips. 24 h after doxycycline induction, the cells were incubated with 10 μM 5-ethynyl-2-deoxyuridine (EdU, Jena Bioscience) for 15 min, and directly fixed with 4% paraformaldehyde for 15 min. Fixed cells were permeabilized with 1X PBS containing 0.5% Triton-X. The cells were blocked with 3% BSA containing 0.3% Triton X-100, and subsequently incubated for 30 min with EdU Click-iT reaction cocktail (50 mM Tris–HCl (pH 7.6), 150 mM NaCl, 1 μM picolyl azide 5/6-FAM (#CLK-1180, Jena Bioscience), 4 mM $CuSO_4$ and 2 mg/ml sodium-L-ascorbate). The cells were mounted using ProLong™ Gold Antifade Mountant with DAPI (Invitrogen) and EdU-positive nuclei were quantified in ImageJ (75) using a custom-built macro.

γH2AX foci

Cells were seeded on 12 mm coverslips and 24 h after doxycycline induction, cells were either mock treated or irradiated with ionizing radiation delivered by a YXlon X-ray generator (YXlon International, 200 KV, 6 mA, 3 Gy). Cells were fixed 1 h after irradiation with 4% paraformaldehyde and permeabilized with 1× PBS containing 0.5% Triton-X. Cells were blocked with 100 mM glycine in 1× PBS for 10 min. The cells were then incubated with an antibody against γH2AX (Table 2) for 2 h, followed by incubation with the secondary antibody (Table 2) for 1 h. Cells were mounted using ProLong™ Gold Antifade Mountant with DAPI (Invitrogen) and γH2AX foci per cell were evaluated in ImageJ (75) using a custom-built macro that enabled automatic and objective analysis of the foci as described previously (76).

HI-NESS-expressing cell lines: microscopy

Images of fixed samples were acquired on a Zeiss AxioImager M2 widefield fluorescence microscope equipped with 63× PLAN APO (1.4 NA) oil-immersion objectives (Zeiss) and an HXP 120 metal-halide lamp used for excitation. Fluorescent probes were detected using the following filters: DAPI (excitation filter: 350/50 nm, dichroic mirror: 400 nm, emission filter: 460/50 nm), GFP (excitation filter: 470/40 nm, dichroic mirror: 495 nm, emission filter: 525/50 nm), Alexa 555 (excitation filter: 545/25 nm, dichroic mirror: 565 nm, emission filter: 605/70 nm), Alexa 647 (excitation filter: 640/30 nm, dichroic mirror: 660 nm, emission filter: 690/50 nm). Images were recorded using ZEN 2012 (Blue edition, Version 1.1.0.0) software and analyzed in ImageJ (1.48v) (75).

HI-NESS-expressing cell lines: cell cycle analysis

150 000 cells were seeded in six-well plates and 24 h later treated with doxycycline. 24 h after the doxycycline induction, the cells were collected by trypsinization and fixed in 80% ice-cold ethanol. The DNA was stained with 50 μg/ml propidium iodide in the presence of 0.1 mg/ml RNaseA and 0.05% Triton X-100. The fluorescence intensity was measured by flow cytometry (Guava, Millipore) and used to determine cell cycle phase distribution (Flowing software 2).

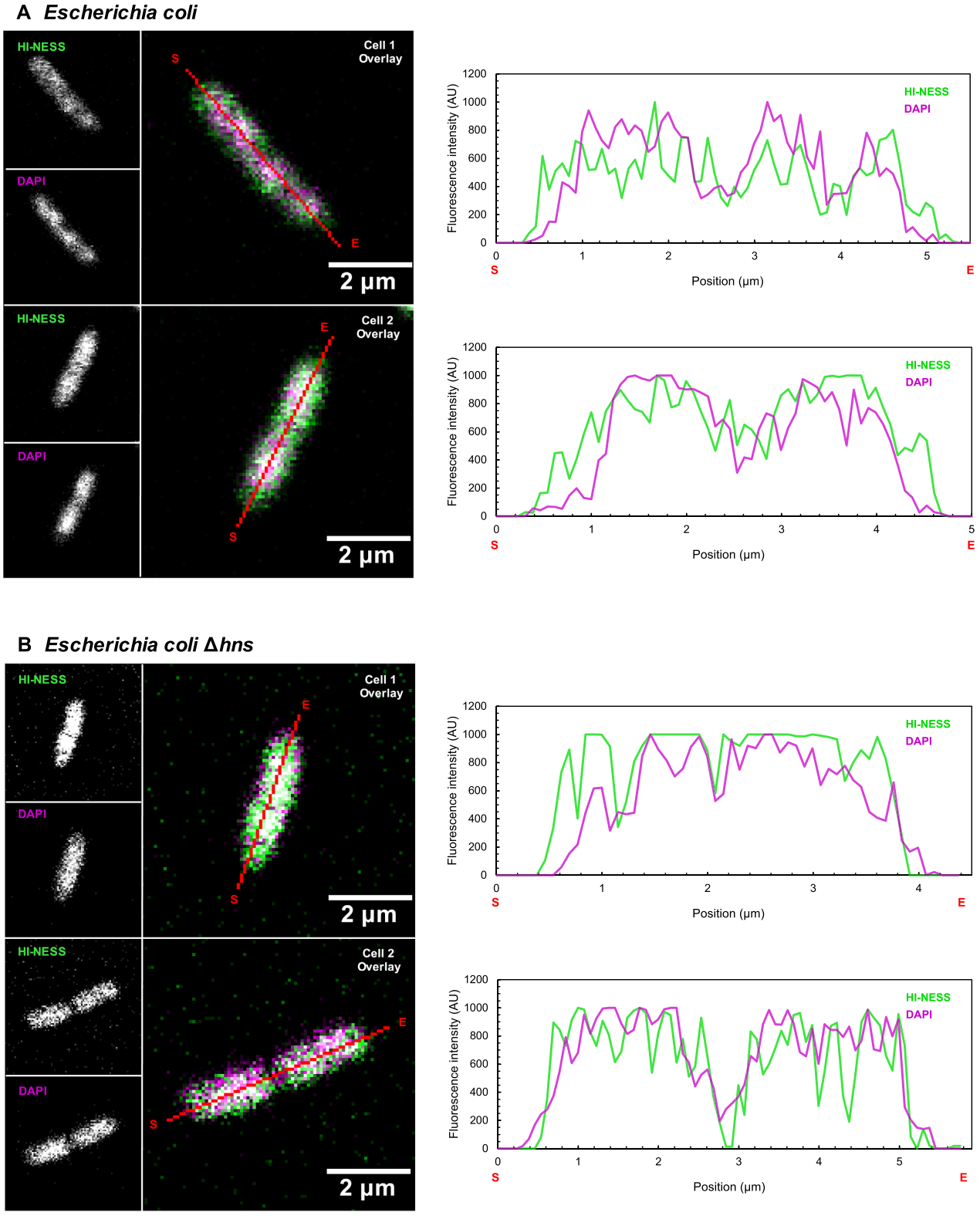

Figure 1. HI-NESS distribution in wild-type *Escherichia coli* and *E. coli* Δ*hns* (*Confocal microscopy, single Z-plane*). (**A**) HI-NESS (green) labels the nucleoid in wild-type *E. coli* where its distribution correlates—albeit poorly—with the DAPI signal (magenta). HI-NESS also distributes in the cytoplasm of these cells, decreasing the signal-to-noise ratio and the applicability of HI-NESS as a DNA label in wild-type *E. coli*. (**B**) In *E. coli* Δ*hns*, HI-NESS localises in the nucleoid. Line scans across *E. coli* and *E. coli* Δ*hns* cells are marked in red with start and end positions indicated with S and E, respectively. A white signal in the Overlay images represents colocalization.

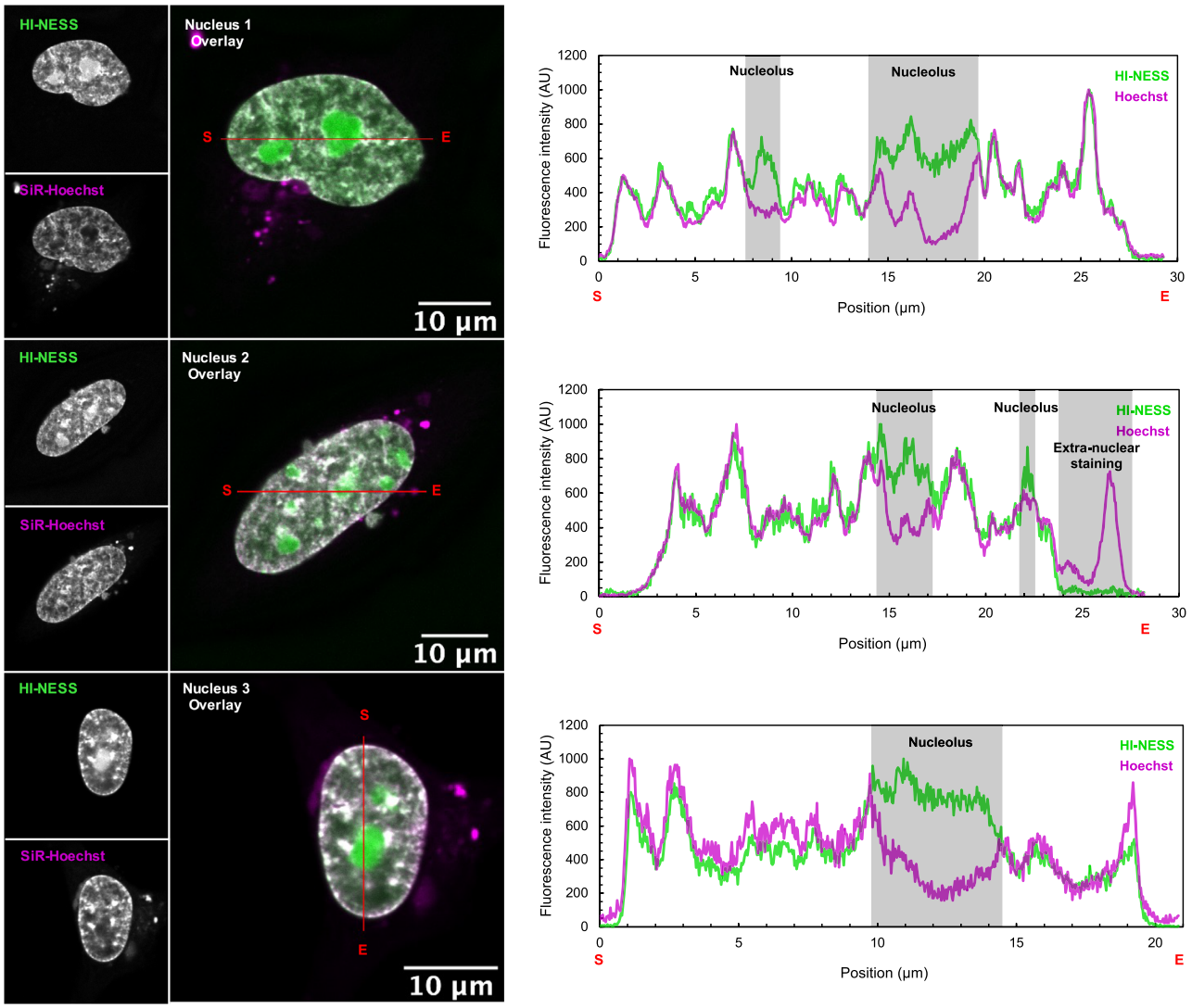

Figure 2. HI-NESS labels chromosomes in HeLa cells in culture (*Confocal microscopy, single Z-plane*). Line scans (marked in red with start and end positions indicated with S and E, respectively) across nuclei of HeLa cells co-stained with HI-NESS (green) and SiR-Hoechst (magenta) highlight the overlap between the distributions of the two DNA labels. However, HI-NESS also accumulates in nucleoli due to high levels of the protein in the nucleus and its affinity for RNA as detected in *in vitro* studies (Supplementary Figure S4; Supplementary Table S1).

HI-NESS imaging in zebrafish embryos and larvae

Zebrafish lines used in this study (AB/TL wild types) were handled in compliance with local animal welfare regulations, as overseen by the Animal Welfare Body of Leiden University (License number: 10612) and maintained according to standard protocols (http://zfin.org/). All experiments were done on embryos or larvae up to 5 days post-fertilization (dpf), that had not yet reached the free-feeding stage. Embryos/larvae were kept in egg water (60 µg/ml Instant Ocean sea salts) at 28.5°C and anesthetized with 0.02% ethyl 3-aminobenzoate methanesulfonate (Tricaine, Sigma-Aldrich) before imaging and fixation.

To achieve mosaic expression of HI-NESS and the mEos3.2 control, 25–50 pg of pRD188 or pRD190 (Table 1) in 1× Danieau buffer (58 mM NaCl, 0.7 mM KCl, 0.4 mM $MgSO_4$, 0.6 mM $Ca(NO_3)_2$ and 5.0 mM HEPES (pH 7.6)) was microinjected into zebrafish embryos at the one-cell stage. After 24 h, the embryos were screened for fluorescence using a Leica MZ16FA stereo fluorescence microscope. For co-staining with DAPI, larvae expressing HI-NESS or the mEos3.2 control were fixed with 4% PFA in 1× PBS at 4°C overnight. Fixed larvae were washed with 1× PBS and stained with DAPI (Sigma-Aldrich) at a final concentration of 100 µg/ml in 1× PBS. Fixed or live embryos of 2 dpf were mounted with 1.5% low melting point agarose (SERVA) in egg water and imaged using a Leica TCS SPE or SP8 confocal microscope with a 40X water immersion objective (NA 0.8) and excited by 405, 488 or 532 nm laser lines.

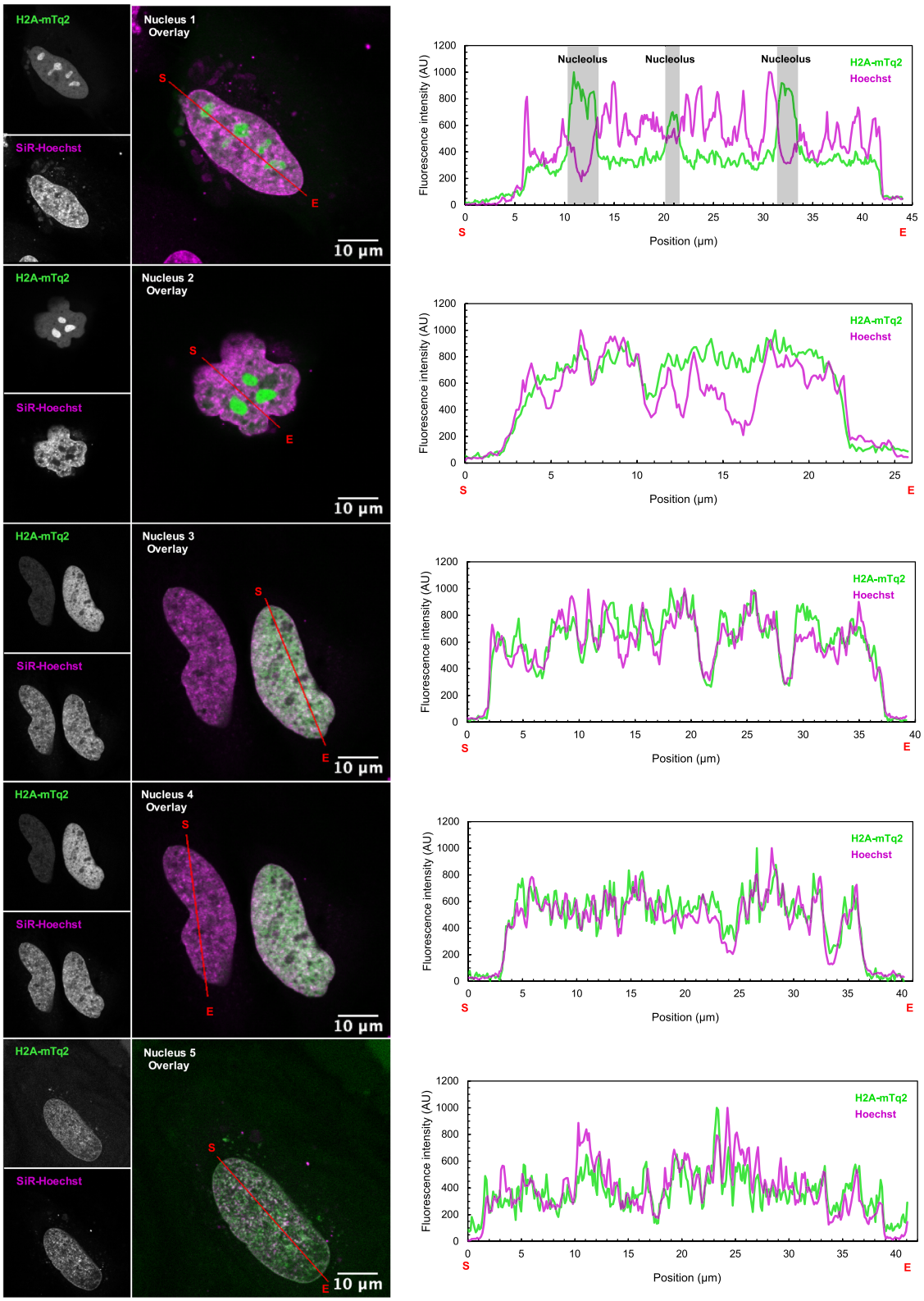

Figure 3. The overlap between H2A-mTurquoise2 (green) and SiR-Hoechst (magenta) signals in HeLa cells (*Confocal microscopy, single Z-plane*). Nuclei 1 and 2: Extensive nucleolar accumulation of H2A-mTurquoise2 (H2A-mTq2) drowns its fluorescent signal over the rest of the nucleus. Line scans (marked in red with start and end positions indicated with S and E, respectively) across such nuclei show that the H2A-mTq2 signal only recapitulates that of SiR-Hoechst when the line scan does not cross a nucleolus. Nuclei 3, 4, and 5: in cells expressing low levels of H2A-mTq2 (nuclei 3 and 4), and in nuclei with no visible nucleoli (nucleus 5) the distribution of the SiR-Hoechst and H2A-mTq2 signals are comparable.

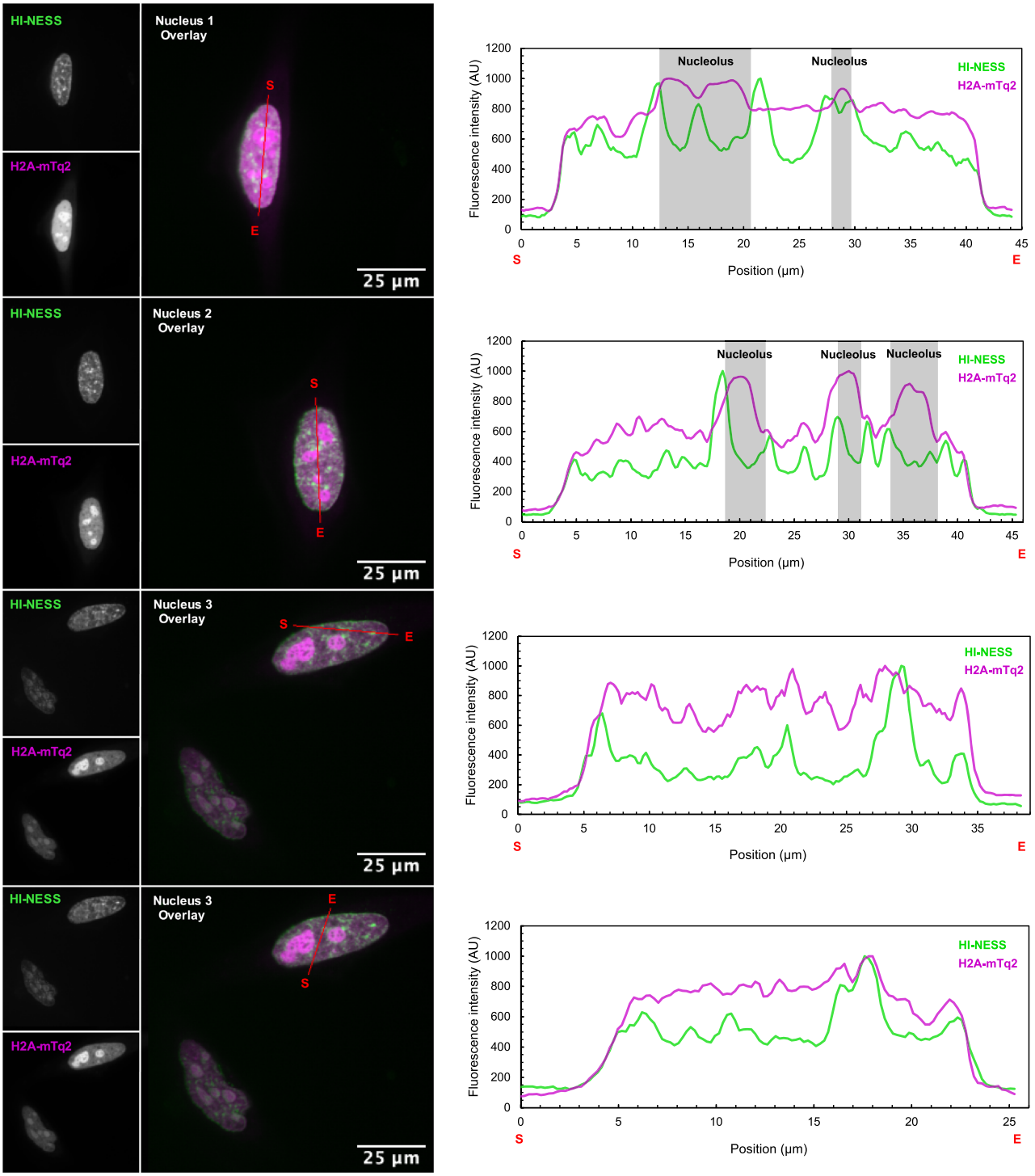

Figure 4. The distribution of mEos3.2-tagged HI-NESS (green) and H2A-mTq2 (magenta) in the nuclei of HeLa cells in culture (*Spinning disk microscopy, single Z-plane*). In HeLa cells co-expressing mEos3.2-tagged HI-NESS and H2A-mTq2, the fluorescently-labelled histone exhibits extensive nucleolar retention, and consequently, stains the chromosomes with a low signal-to-noise ratio. The decreased nucleolar accumulation of HI-NESS allows chromosomes to be visualised with a higher signal-to-noise ratio. Line scans (marked in red with start and end positions indicated with S and E, respectively) across these nuclei highlight the effect of nucleolar retention on the signal over the rest of the nucleus.

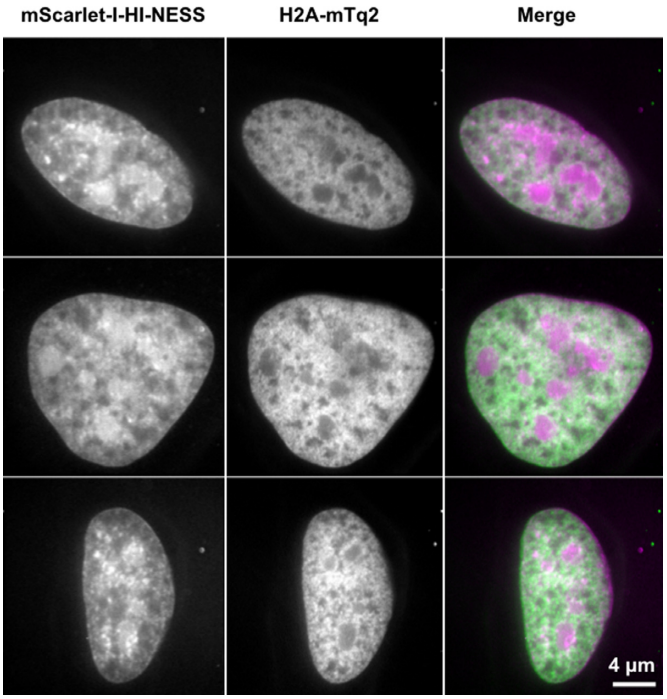

Figure 5. The distribution of mScarlet-I-HI-NESS (magenta) and H2A-mTq2 (green) in the nuclei of HeLa cells expressing lower levels of the fluorescent proteins (*Spinning disk microscopy, single Z-plane*). The distribution of the mScarlet-I-HI-NESS signal (left) in the nuclei recapitulates that of earlier experiments (Figures 2 and 4), with the label showing some nucleolar accumulation, and the presence of dense foci. The distribution of H2A-mTq2 (middle), on the other hand, differs (Figures 3 and 4). H2A-mTq2 does not accumulate in the nucleoli of cells expressing lower levels of the protein. H2A-mTq2 also exhibits a visibly different distribution compared to that of mScarlet-I-HI-NESS, with a relatively homogeneous signal over the nucleus and the apparent lack of the dense foci observed with HI-NESS. The discrepancy may arise from the homogeneous binding of H2A-mTq2 along the chromosome, in contrast to the preferential binding of Hoechst and HI-NESS to AT-rich sequences (Supplementary Figure S4; Supplementary Table S1) (4–6).

RESULTS AND DISCUSSION

HI-NESS is outcompeted by native H-NS in binding to chromosomal DNA

We engineered HI-NESS by preparing a fusion construct of mEos3.2, a photo-switchable fluorescent protein, to the N-terminus of an *Escherichia coli* H-NS truncation comprising residues 80–137 of the wild-type protein. In this construct, mEos3.2 allows visualization of the DNA-labelling protein in diffraction-limited and, potentially, super-resolution microscopy, residues 96–137 of H-NS fold into a DNA-binding domain, and H-NS residues 80–95 form a linker that separates the aforementioned moieties to prevent steric clashes and protein misfolding. In this construct, mEos3.2 was fused to the DNA-binding domain of H-NS as opposed to full-length H-NS, to achieve a high DNA dissociation constant (77), and to prevent the potential multimerization of HI-NESS that may arise from the presence of an oligomerisation domain (65). These features are expected to make the DNA-labelling protein less perturbing to genomic transactions in the cell. To verify this, the distribution of HI-NESS was tested in *E. coli*, where the protein was ectopically expressed from a plasmid. HI-NESS was expected to be outcompeted by native H-NS in binding to chromosomal DNA, while DNA labelling with a high signal-to-noise ratio was expected in the absence of endogenous H-NS. Indeed, HI-NESS distributed in both, the nucleoid and the cytoplasm of wild-type *E. coli* (Figure 1A), whereas the protein was localised in the nucleoid of *E. coli* Δ*hns* (Figure 1B). This observation also implies that HI-NESS is not a suitable DNA stain for use in *E. coli*. HI-NESS is also unsuitable in bacteria that express H-NS-like proteins that tend to show a preference for AT-rich sequences (78,79). The distribution of HI-NESS and that of mEos3.2 without the DNA binding moiety in *Mycobacterium marinum*, an organism that expresses the H-NS-like nucleoid-associated protein Lsr2, was indistinguishable (Supplementary Figure S1).

HI-NESS labels chromosomes in eukaryotic cells

The DNA-binding properties of HI-NESS make it an excellent candidate for chromosome labelling in eukaryotic cells. A pcDNA3.1 (+) vector was used to transiently express HI-NESS flanked by a pair of SV40 T-antigen derived nuclear localisation signals (NLSs) in HeLa, BOEC, and U2OS cells. The fluorescence signal appeared as several discrete and dense foci in nuclei (Figure 2, Supplementary Figure S2) that overlapped with the SiR-Hoechst signal (Figure 2). Such foci were not visible when the cells expressed NLS-mEos3.2-NLS lacking the H-NS DNA-binding domain (Supplementary Figure S3). HI-NESS also accumulated in nucleoli – structures that contain little DNA, but tend to be enriched in RNA and protein (Figure 2, Supplementary Figure S2). The accumulation is expected to be largely non-specific and to occur due to high levels of HI-NESS in the nucleus since HI-NESS lacks detectable nucleolar localisation/retention signals (NoRSs) (80,81), and the SV40 T-antigen derived NLS cannot drive nucleolar accumulation of proteins (82). However, the affinity of HI-NESS for RNA in *in vitro* assays indicates that the accumulation may partly be due to RNA labelling (Supplementary Figure S4; Supplementary Table S1).

We evaluated the use of HI-NESS as an alternative to fluorescently-tagged histone proteins to label eukaryotic chromosomes. H2A-mTurquoise2 (H2A-mTq2) (83) was transiently expressed in HeLa cells and the nuclei were co-stained with SiR-Hoechst. H2A-mTq2 exhibited extensive nucleolar accumulation that drowned the fluorescence signal over the rest of the nucleus, consequently, reducing the signal-to-noise ratio for chromosome visualisation (Figure 3, nuclei 1 and 2). Nucleolar accumulation of histones has also been observed for fluorescently-labelled H2B, driven by the presence of a NoRS in the protein's nuclear localisation signal (84). NoRS tend to be enriched in positively-charged (basic) amino acids that facilitate electrostratic interactions with the negatively-charged (acidic) contents of the nucleolus (84). In the case of H2A-mTq2, nucleolar accumulation occurs in the absence of a detectable NoRS in the construct (80,81), and may be promoted by the inherent basicity of the protein. Nucleolar accumulation of fluorescently-tagged histones is generally observed in cells where the fusion protein is transiently expressed. This arises as a result of high levels of transient expression and the lack of a sufficient num-

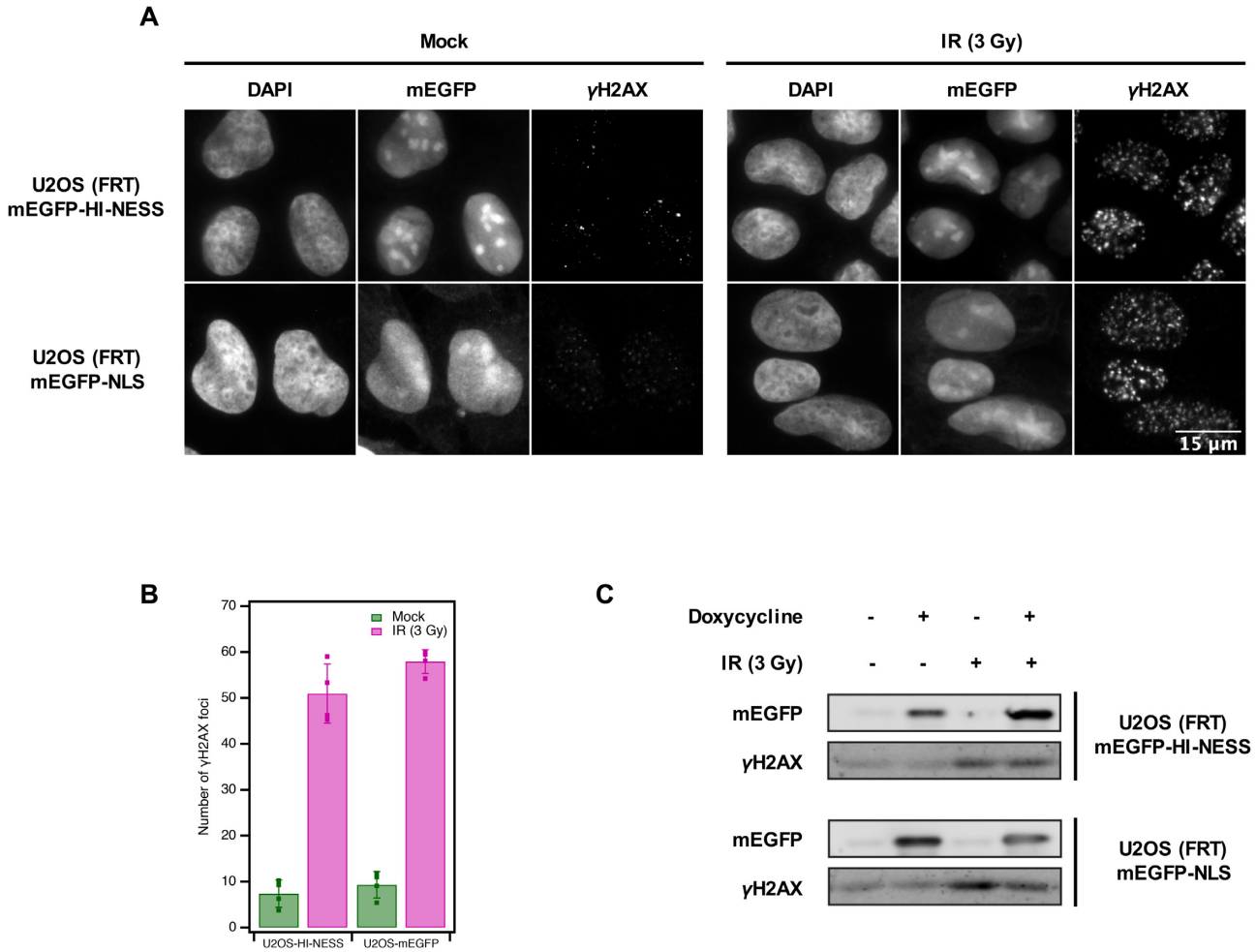

Figure 6. HI-NESS does not induce increased rates of DNA damage. The induction of γH2AX—a DNA damage biomarker—in U2OS (FRT) cells stably expressing mEGFP-HI-NESS is comparable to cells expressing mEGFP-NLS as visualised by microscopy (Wide field microscopy, single Z-plane) (Panel A, left). On average, 7.4 ± 3.0 γH2AX foci were detected in U2OS cells expressing mEGFP-HI-NESS cells, compared to 9.3 ± 2.9 foci with mEGFP-NLS expression (Panel B, green). γH2AX is induced when the cells are treated with 3 Gy ionizing radiation (IR) (Panel A, right), 51.0 ± 6.4 γH2AX foci appear in U2OS (FRT) mEGFP-HI-NESS cells, and 57.9 ± 2.6 in U2OS (FRT) mEGFP-NLS cells (Panel B, magenta). Panel C: Western blot shows that γH2AX induction is unaffected by the expression of HI-NESS. Furthermore, γH2AX induction and hence, the DNA damage response, following IR treatment is not affected by HI-NESS.

ber of cell cycles during which the fluorescently-tagged histone can be deposited in chromosomes. We occasionally observed cells with minimal, if any, nucleolar accumulation of H2A-mTq2 (Figure 3, nuclei 3 and 4). These cells expressed low levels of H2A-mTq2 as inferred from low fluorescence in the mTurquoise2 channel. In these cases, line scans across nuclei show that the H2A-mTq2 signal tends to recapitulate the SiR-Hoechst signal (Figure 3, nuclei 3 and 4). A similar observation was made for nuclei that lacked visible nucleoli (Figure 3, nucleus 5).

We transiently co-expressed HI-NESS (with mEos3.2 as a fluorescent label) and H2A-mTq2 in HeLa cells to compare the distribution of the DNA labels in the same nuclei. The study reproduced the extensive nucleolar accumulation of H2A-mTq2 (Figure 4) – a circumstance that decreases the signal-to-noise ratio for chromosome visualisation. In comparison, chromosomes were observed with a high signal-to-noise ratio in the HI-NESS channel, with the DNA label exhibiting decreased nucleolar accumulation (Figure 4) compared to cells in which only HI-NESS was ectopically expressed (Figure 2).

The green state of mEos3.2 used to visualise HI-NESS in our experiments has a half-life of 12.55 s (85) and bleaches rapidly. As a consequence, often only those cells expressing high levels of the HI-NESS and H2A-mTq2 were imaged. When mEos3.2 was replaced with mScarlet-I, a non-photoswitchable fluorophore with a fluorescence half-life of 190 s in a spinning disk confocal microscopy set-up (86), cells expressing much lower levels of mScarlet-I-HI-NESS and H2A-mTq2 were successfully imaged (Figure 5). In these cells, the distribution of the mScarlet-I-HI-NESS signal recapitulated that of earlier experiments (Figures 2 and 4): some nucleolar accumulation, and the presence of dense foci. The distribution of H2A-mTq2 (Figure 5), on the other hand, differed from nuclei where the protein exhibited high levels of expression (Figure 3, nuclei 1 and 2 and Figure 4). H2A-mTq2 did not accumulate in nucleoli (Figure 5 and Figure 3, nuclei 3 and 4). Here, H2A-mTq2 also ex-

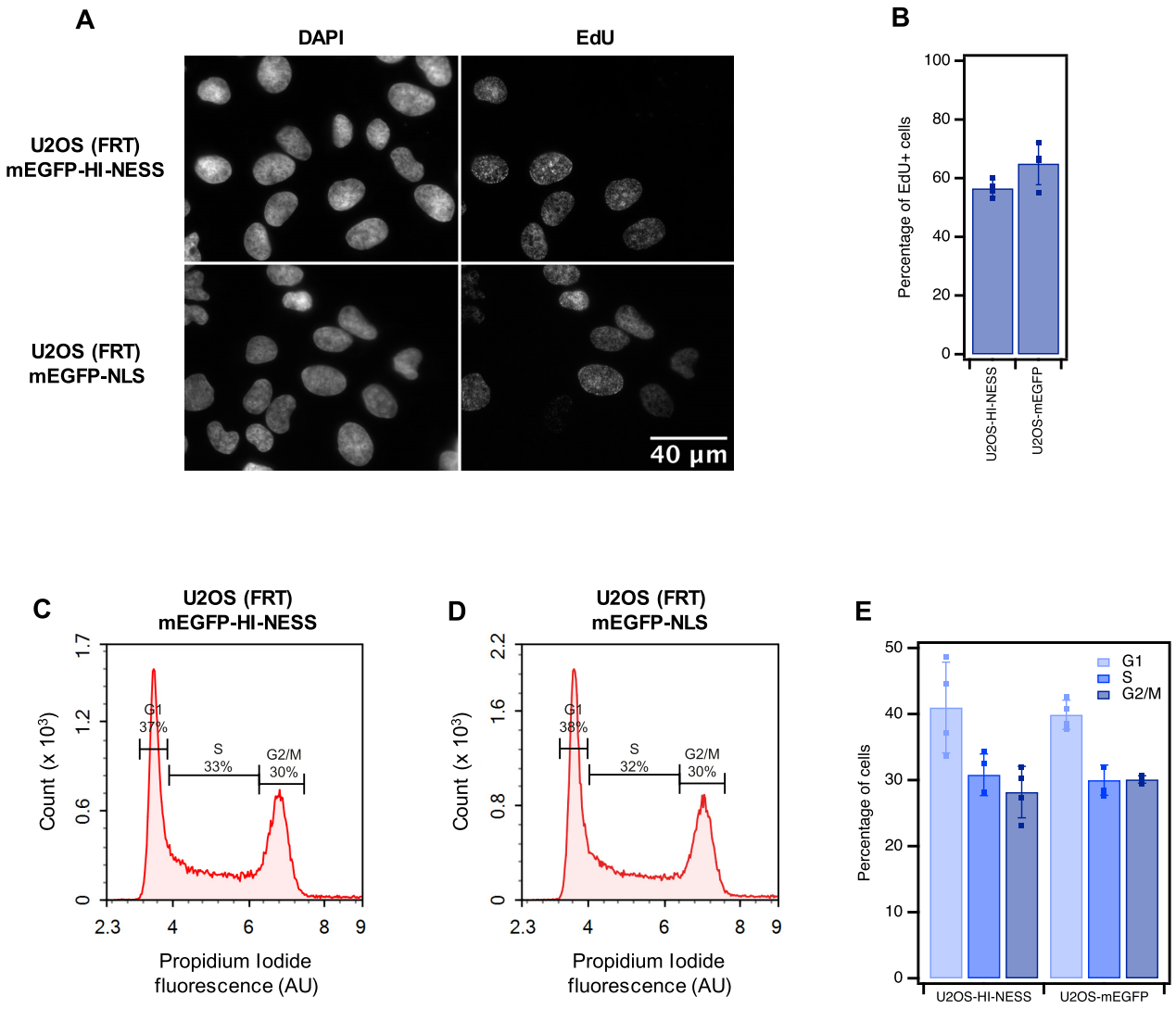

Figure 7. HI-NESS does not interfere with cell cycle progression. Panel **A**: U2OS (FRT) cells in the S-phase were visualised (Wide field microscopy, single *Z*-plane) by pulse-labelling the cells with EdU and 'clicking' the molecule to 5/6-FAM. Panel **B**: 56.6 ± 2.9% of U2OS (FRT) cells expressing mEGFP-HI-NESS (U2OS-HI-NESS) occur in the S-phase of the cell cycle compared to 65 ± 7.2% of cells expressing mEGFP-NLS (U2OS-mEGFP). Flow cytometry of propidium iodide-labelled cells (Panels **C**–**E**) detects 37% of U2OS-HI-NESS cells in the G1 phase of the cell cycle, 33% in the S phase and 30% in the G2/M phase (Panels C and E). Of the U2OS-mEGFP cells, 38% occur in the G1 phase, 32% in the S phase and 30% in the G2/M phase (Panels D and E).

hibited a visibly different distribution compared to that of mScarlet-I-HI-NESS (Figure 5), showing a rather homogeneous distribution in the nucleus and the apparent lack of the discrete and dense foci characteristic of eukaryotic nuclei labelled with HI-NESS or SiR-Hoechst. The discrepancy may arise from the homogeneous binding of H2A-mTq2 along the chromosome, in contrast to the preferential binding of Hoechst and HI-NESS to AT-rich sequences (Supplementary Figure S4; Supplementary Table S1) (4–6). Indeed, line scans across the nuclei of cells expressing H2A-mTq2—particularly those that do not cross nucleolar regions — also show a relatively homogeneous H2A-mTq2 signal (Figure 3, Nucleus 2 and Figure 4, Nucleus 3), compared to the Hoechst (Figure 3, nucleus 2) and HI-NESS (Figure 4, nucleus 3) signals from the same nucleus.

HI-NESS does not cause increased rates of DNA damage, affect the recruitment of γH2AX to sites of DNA damage, or interfere with cell cycle progression

DNA-labelling agents can cause DNA damage and interfere with cell cycle progression. To test whether HI-NESS-based DNA-labelling produces such an effect, a U2OS (FRT) cell line stably expressing NLS-mEGFP-H-NSdbd-NLS from a doxycycline-inducible promoter (U2OS-HI-NESS) was generated using the Flp-In/T-REx system. The expression of mEGFP-HI-NESS in cells of this cell line was verified with microscopy (Supplementary Figure S5). U2OS-HI-NESS was evaluated for changes in the rates of DNA damage, the induction of γH2AX at sites of DNA damage, and in cell cycle progression. A U2OS (FRT) cell

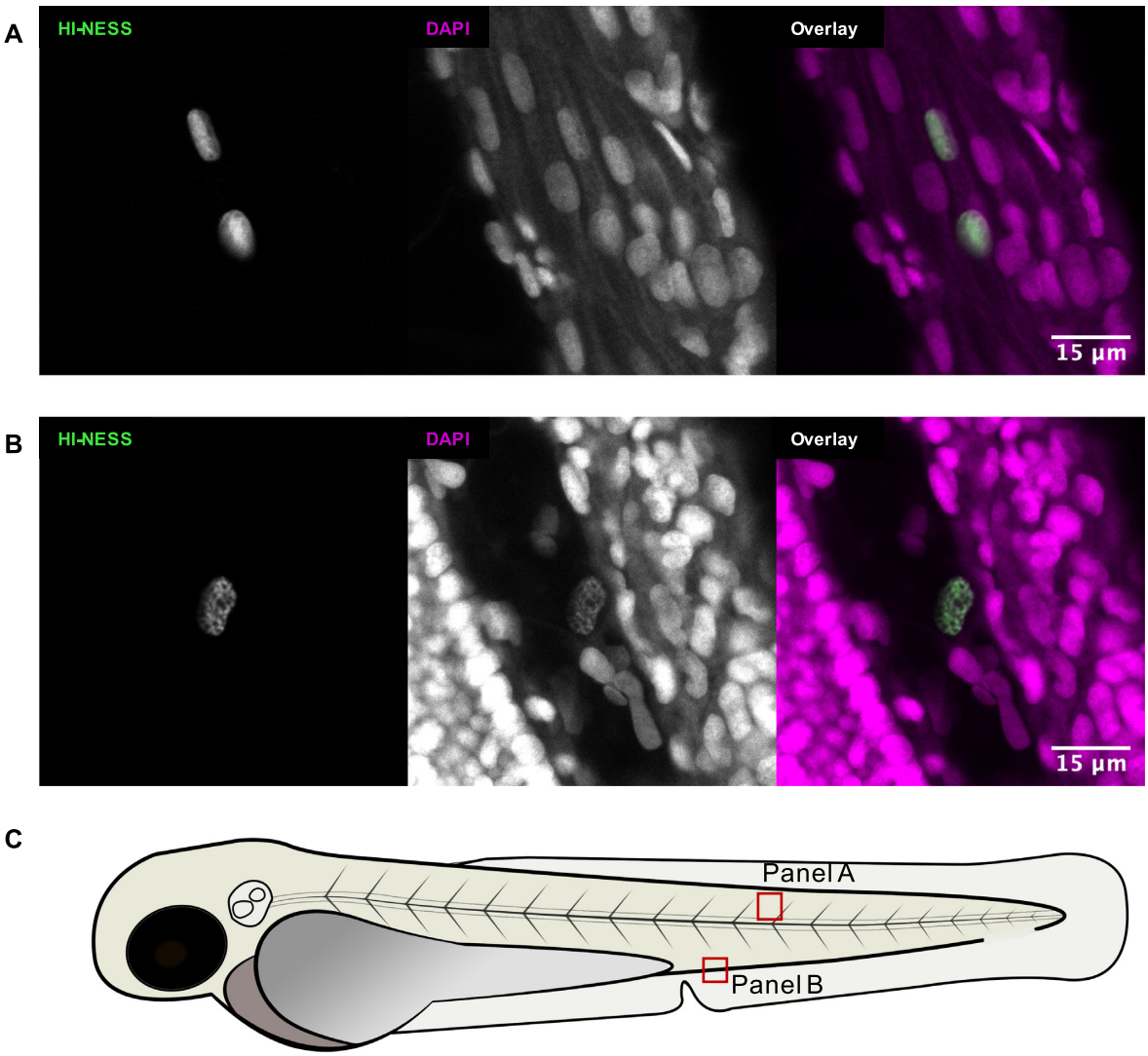

Figure 8. HI-NESS labels chromosomes in zebrafish larvae (confocal microscopy, single *Z*-plane). The distribution of the mEos3.2 signal (green) in nuclei of zebrafish larvae overlapped with that of DAPI (magenta). Nucleolar accumulation of HI-NESS was not observed. (**A**) Striated muscle cells (Trunk); (**B**) from left to right: trunk, blood vessel, yolk extension. The HI-NESS labelled cell is within a blood vessel. The approximate locations in the zebrafish embryo at which (A) and (B) were imaged is provided in (**C**).

line expressing mEGFP-NLS upon doxycycline induction (U2OS-mEGFP) was used as a control.

The rates of DNA damage were determined using γH2AX—a DNA damage biomarker (87). γH2AX is a phosphorylated variant of the H2AX histone protein that forms foci at sites of DNA damage—such as double-stand breaks (DSBs)—triggering the recruitment of DNA repair proteins to these sites (88). We studied the effect of HI-NESS on DNA damage by visualising γH2AX foci with immunofluorescence. Generally, 7.4 ± 3.0 γH2AX foci were observed in U2OS-HI-NESS cells, compared to 9.3 ± 2.9 foci in U2OS-mEGFP (Figures 6A and B; Supplementary Table S2). Upon treatment with ionizing radiation (IR) to induce DSBs, 51.0 ± 6.4 γH2AX foci appear in U2OS-HI-NESS cells, and 57.9 ± 2.6 in U2OS-mEGFP cells (Figure 6A and B; Supplementary Table S2). The increase in γH2AX upon IR treatment was verified by western blot (Figure 6C). Collectively, the results indicate that DNA labelling with HI-NESS does not trigger increased rates of DSBs, or affect the induction of γH2AX to these sites.

Potential changes in cell cycle progression were evaluated with EdU pulse-labelling, and with flow cytometry of fixed cells labelled with propidium iodide. EdU is incorporated in place of thymidine during DNA replication, and can be 'clicked' to an organic fluorophore to visualise cells in the S phase (89). 56.6 ± 2.9% of EdU-pulse labelled U2OS-HI-NESS cells showed incorporation of the thymidine analogue in replicating chromosomes, comparable to 65 ± 7.2% of U2OS-mEGFP cells (Figure 7A and B; Supplementary Table S3). This highlights that the percentage of cells in the S-phase is not affected by the HI-NESS-based DNA-labelling strategy. Next, fixed U2OS-HI-NESS and U2OS-mEGFP cells labelled with propidium iodide were used to determine the distribution of cells in the G1, S, and

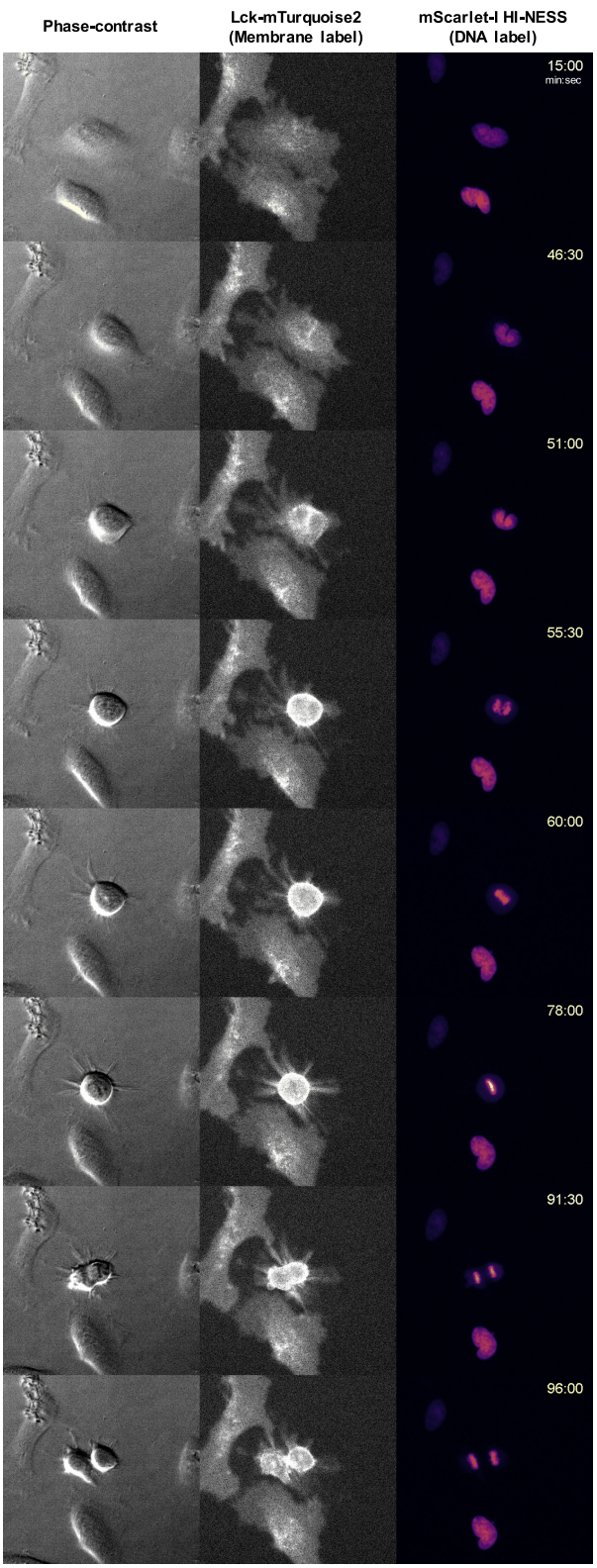

Figure 9. HI-NESS can be used to visualise chromosome dynamics during the cell cycle (wide field microscopy, single *Z*-plane). A time-lapse of a dividing HeLa cell (Movie S8) shows that HI-NESS remains bound to the chromosome during mitosis. From left to right: Phase contrast image, Lck-mTurquoise2 (membrane label), mScarlet-I-HI-NESS (DNA label).

G2/M phases of the cell cycle using flow cytometry. The fluorescence intensity of propidium iodide is a measure of the DNA content of a cell and hence representative of its stage in the cell cycle. 37% of U2OS-HI-NESS cells were determined to be in the G1 phase of the cell cycle, 33% in the S phase and 30% in the G2/M phase (Figure 7C and E; Supplementary Table S4). In comparison, the distribution of U2OS-mEGFP cells across the G1, S, and G2/M phases was 38%, 32% and 30%, respectively (Figure 7D and E; Supplementary Table S4). At 32% and 33%, the fraction of cells determined to be in the S phase with flow cytometry is lower than that from EdU pulse-labelling. The discrepancy arises since EdU pulse labelling visualises active replication forks to determine if a cell is in the S phase while flow cytometry of propidium iodide-labelled cells predicts S-phase from the fluorescence intensity measurement of the cell. Nevertheless, the results show that HI-NESS does not perturb cell cycle progression in U2OS (FRT) cells.

HI-NESS as a DNA label in zebrafish larvae

The feasibility of chromosomal DNA staining in whole organisms using HI-NESS was investigated in zebrafish. HI-NESS and the NLS-mEos3.2-NLS control were expressed in zebrafish from pcDNA3.1(+) vectors microinjected into the embryos at the one-cell stage. The distribution of the fluorophores was visualised using confocal laser scanning microscopy in fixed zebrafish larvae co-stained with DAPI. Predictably, HI-NESS was detected in cell nuclei where its distribution overlapped with that of DAPI (Figure 8, movies S1–S4). Interestingly, nucleolar accumulation of HI-NESS was not observed. This may be due to a lower expression of HI-NESS. However, it also indicates that while HI-NESS exhibits a comparable affinity for RNA and DNA *in vitro* (Supplementary Figure S4, Supplementary Table S1), HI-NESS might preferentially bind to DNA in an *in vivo* system. In zebrafish larvae expressing NLS-mEos3.2-NLS lacking the H-NS DNA-binding domain, the fluorescent protein accumulated in nucleoli and distributed uniformly over the non-nucleolar regions of the nucleus. Evidently, the mEos3.2 signal did not recapitulate the distribution of DAPI (Supplementary Figure S6, movies S5–S7).

Zebrafish larvae exhibited a mosaic expression of HI-NESS and NLS-mEos3.2-NLS in our experiments (Supplementary Figure S7) owing to the microinjection of the pcDNA3.1(+) vector into embryos at the one-cell stage. For constitutive HI-NESS expression in an animal model, the Tol2 transposon-based gene insertion system (reviewed in (90,91)), or CRISPR-Cas9-mediated knock-in (reviewed in (92)) may be used to integrate the HI-NESS gene into the genome. Constructs with the HI-NESS gene placed downstream of a cell-type-specific promoter may also be designed to selectively label nuclei in a live animal model.

HI-NESS is customisable

HI-NESS is a modular protein comprised of fluorescent, DNA-binding, and, optionally, organelle-targeting segments. The protein domains forming these segments can potentially be switched out for others exhibiting similar properties. We have generated a range of HI-NESS labels

where mEos3.2 has been swapped for non-photoswitchable fluorescent proteins (Table 1). In eukaryotes, HI-NESS and its variants can be used to visualise chromosome dynamics during the cell cycle at a high spatial and temporal resolution (Figure 9, Supplementary Figure S8; movie S8), and follow the movements of nuclei in a live animal model (movie S9). The addition of organelle-targeting/localization signals could be exploited to specifically label nuclear, mitochondrial, or chloroplast DNA. In prokaryotes, we predict that HI-NESS can be used to visualise the chromosome in bacteria naturally lacking H-NS and H-NS-like proteins. The H-NS-based DNA-binding module can also be replaced with archaeal DNA-binding domains or stable variants evolved from the H-NS-based module to study chromosome dynamics in extremophiles.

CONCLUSION

We have designed a minimally-perturbing, DNA-labelling protein to visualise chromosomes in eukaryotic cells in culture and in live animal models. We have shown that in these systems, the distribution of the label—HI-NESS—overlaps with that of traditional DNA labels such as DAPI and SiR-Hoechst. HI-NESS offers an alternative to fluorescently labelled histone proteins, especially in applications that need to avoid over-expression of histone proteins or for experiments that require a stain compatible with live-cell imaging with a distribution that closely mimics that of organic DNA dyes.

DATA AVAILABILITY

Fiji/ImageJ are open-source image processing programs made available by the National Institutes of Health (NIH), Bethesda, USA.

Prism8 is an analysis and graphing software developed by GraphPad Software, San Diego, USA.

Flow Cytometry data have been made available via the FlowRepository under the Repository ID: FR-FCM-Z3NP.

Microscopy data have been made available via the 4TU Repository (DOI:10.4121/14464842).

SUPPLEMENTARY DATA

Supplementary Data are available at NAR Online.

ACKNOWLEDGEMENTS

The authors would like to thank Dr Monika Timmer for discussions on protein purification and Prof. Theodorus W.J. Gadella for plasmids mNeonGreen-C1 and mScarlet-I-C1.

FUNDING

Netherlands Organization for Scientific Research [VICI 016.160.613 to R.T.D., ENW-M OCENW.KLEIN.090 to M.S.L., VIDI ALW.016.161.320 to M.S.L., ALWOP.306 to E.M.]; FOM Foundation for Fundamental Research on Matter program ‘Crowd management: the physics of genome processing in complex environments’ (to R.T.D.); Human Frontier Science Program (HFSP) [RGP0014/2014 to R.T.D.]. Funding for open access charge: Nederlandse Organisatie voor Wetenschappelijk Onderzoek VICI Grant [016.160.613].

Conflict of interest statement. None declared.

REFERENCES

1. Dame,R.T., Rashid,F.Z.M. and Grainger,D.C. (2020) Chromosome organization in bacteria: mechanistic insights into genome structure and function. *Nat. Rev. Genet.*, **21**, 227–242.
2. Dame,R.T. and Tark-Dame,M. (2016) Bacterial chromatin: converging views at different scales. *Curr. Opin. Cell Biol.*, **40**, 60–65.
3. Yu,M. and Ren,B. (2017) The three-dimensional organization of mammalian genomes. *Annu. Rev. Cell Dev. Biol.*, **33**, 265–289.
4. Banerjee,D. and Pal,S.K. (2008) Dynamics in the DNA recognition by DAPI: exploration of the various binding modes. *J. Phys. Chem. B*, **112**, 1016–1021.
5. Trotta,E., D’Ambrosio,E., Ravagnan,G. and Paci,M. (1996) Simultaneous and different binding mechanisms of 4′,6-diamidino-2-phenylindole to DNA hexamer (d(CGATCG))2: A 1H NMR study. *J. Biol. Chem.*, **271**, 27608–27614.
6. Bailly,C., Colson,P., Hénichart,J. and Houssier,C. (1993) The different binding modes of hoechst 33258 to DNA studied by electirc linear dichroism. *Nucleic Acids Res.*, **21**, 3705–3709.
7. Nakayama,A., Bianco,A.C., Zhang,C.Y., Lowell,B.B. and Frangioni,J. V. (2003) Quantification of brown adipose tissue perfusion in transgenic mice using near-infrared fluorescence imaging. *Mol. Imaging*, **2**, 37–49.
8. Nakamura,A., Takigawa,K., Kurishita,Y., Kuwata,K., Ishida,M., Shimoda,Y., Hamachi,I. and Tsukiji,S. (2014) Hoechst tagging: a modular strategy to design synthetic fluorescent probes for live-cell nucleus imaging. *Chem. Commun.*, **50**, 6149–6152.
9. Dasari,M., Lee,S., Sy,J., Kim,D., Lee,S., Brown,M., Davis,M. and Murthy,N. (2010) Hoechst-IR: an imaging agent that detects necrotic tissue in vivo by binding extracellular DNA. *Org. Lett.*, **12**, 3300–3303.
10. Lukinavičius,G., Blaukopf,C., Pershagen,E., Schena,A., Reymond,L., Derivery,E., Gonzalez-Gaitan,M., D’Este,E., Hell,S.W., Gerlich,D.W. *et al.* (2015) SiR-Hoechst is a far-red DNA stain for live-cell nanoscopy. *Nat. Commun.*, **6**, 8497.
11. Bucevičius,J., Keller-Findeisen,J., Gilat,T., Hell,S.W. and Lukinavičius,G. (2019) Rhodamine-Hoechst positional isomers for highly efficient staining of heterochromatin. *Chem. Sci.*, **10**, 1962–1970.
12. Rye,H.S., Yue,S., Wemmer,D.E., Quesada,M.A., Haugland,R.P., Mathies,R.A. and Glazer,A.N. (1992) Stable fluorescent complexes of double-stranded DNA with bis-intercalating asymmetric cyanine dyes: properties and applications. *Nucleic Acids Res.*, **20**, 2803–2812.
13. Van Hooijdonk,C.A.E.M., Glade,C.P. and Van Erp,P.E.J. (1994) TO-PRO-3 iodide: a novel HeNe laser-excitable DNA stain as an alternative for propidium iodide in multiparameter flow cytometry. *Cytometry*, **17**, 185–189.
14. Glazer,A.N. and Rye,H.S. (1992) Stable dye-DNA intercalation complexes as reagents for high-sensitivity fluorescence detection. *Nature*, **359**, 859–861.
15. Schoen,I., Ries,J., Klotzsch,E., Ewers,H. and Vogel,V. (2011) Binding-activated localization microscopy of DNA l. *Nano Lett.*, **11**, 4008–4011.
16. Szczurek,A., Klewes,L., Xing,J., Gourram,A., Birk,U., Knecht,H., Dobrucki,J.W., Mai,S. and Cremer,C. (2017) Imaging chromatin nanostructure with binding-activated localization microscopy based on DNA structure fluctuations. *Nucleic Acids Res.*, **45**, e56.
17. Legant,W.R., Shao,L., Grimm,J.B., Brown,T.A., Milkie,D.E., Avants,B.B., Lavis,L.D. and Betzig,E. (2016) High-density three-dimensional localization microscopy across large volumes. *Nat. Methods*, **13**, 359–365.
18. Spahn,C.K., Glaesmann,M., Grimm,J.B., Ayala,A.X., Lavis,L.D. and Heilemann,M. (2018) A toolbox for multiplexed super-resolution imaging of the E. coli nucleoid and membrane using novel PAINT labels. *Sci. Rep.*, **8**, 14768.

19. Karg,T.J. and Golic,K.G. (2018) Photoconversion of DAPI and Hoechst dyes to green and red-emitting forms after exposure to UV excitation. *Chromosoma*, **127**, 235–245.
20. Zurek-Biesiada,D., Kedracka-Krok,S. and Dobrucki,J.W. (2013) UV-activated conversion of Hoechst 33258, DAPI, and Vybrant DyeCycle fluorescent dyes into blue-excited, green-emitting protonated forms. *Cytom. Part A*, **83 A**, 441–451.
21. Piterburg,M., Panet,H. and Weiss,A. (2012) Photoconversion of DAPI following UV or violet excitation can cause DAPI to fluoresce with blue or cyan excitation. *J. Microsc.*, **246**, 89–95.
22. Szczurek,A.T., Prakash,K., Lee,H.K., Zurek-Biesiada,D.J., Best,G., Hagmann,M., Dobrucki,J.W., Cremer,C. and Birk,U. (2014) Single molecule localization microscopy of the distribution of chromatin using hoechst and DAPI fluorescent probes. *Nucl. (United States)*, **5**, 331–340.
23. Zurek-Biesiada,D., Szczurek,A.T., Prakash,K., Best,G., Mohana,G.K., Lee,H.K., Roignant,J.Y., Dobrucki,J.W., Cremer,C. and Birk,U. (2016) Quantitative super-resolution localization microscopy of DNA in situ using Vybrant® DyeCycle™ Violet fluorescent probe. *Data Br.*, **7**, 157–171.
24. Spielmann,H.P. (1998) Dynamics of a bis-intercalator DNA complex by 1H-detected natural abundance 13C NMR spectroscopy. *Biochemistry*, **37**, 16863–16876.
25. Spielmann,H.P., Wemmer,D.E. and Jacobsen,J.P. (1995) Solution structure of a DNA complex with the fluorescent bis-intercalator TOTO determined by NMR spectroscopy. *Biochemistry*, **34**, 8542–8553.
26. Kamitori,S. and Takusagawa,F. (1992) Crystal structure of the 2:1 complex between d(GAAGCTTC) and the anticancer drug actinomycin D. *J. Mol. Biol.*, **225**, 445–456.
27. Günther,K., Mertig,M. and Seidel,R. (2010) Mechanical and structural properties of YOYO-1 complexed DNA. *Nucleic Acids Res.*, **38**, 6526–6532.
28. Chiang,S.Y., Welch,J., Beerman,T.A. and Rauscher,F.J. (1994) Effects of minor groove binding drugs on the interaction of TATA box binding protein and TFIIA with DNA. *Biochemistry*, **33**, 7033–7040.
29. Störl,K., Störl,J., Zimmer,C. and Lown,J.W. (1993) Minor-groove binders are inhibitors of the catalytic activity of DNA gyrases. *FEBS Lett.*, **317**, 157–162.
30. Straney,D.C. and Crothers,D.M. (1987) Effect of drug–DNA interactions upon transcription initiation at the lac promoter. *Biochemistry*, **26**, 1987–1995.
31. Woynarowski,J.M., McHugh,M., Sigmund,R.D. and Beerman,T.A. (1989) Modulation of topoisomerase II catalytic activity by DNA minor groove binding agents distamycin, Hoechst 33258, and 4′,6-diamidine-2-phenylindole. *Mol. Pharmacol.*, **35**, 177–182.
32. Parolin,C., Montecucco,A., Ciarrocchi,G., Pedrali-Noy,G., Valisena,S., Palumbo,M. and Palu,G. (1990) The effect of the minor groove binding agent DAPI (2-amidino-diphenyl-indole) on DNA-directed enzymes: an attempt to explain inhibition of plasmid expression in Escherichia coli. *FEMS Microbiol. Lett.*, **68**, 341–346.
33. Åkerman,B. and Tuite,E. (1996) Single- and double-strand photocleavage of DNA by YO, YOYO and TOTO. *Nucleic Acids Res.*, **24**, 1080–1090.
34. Tycon,M.A., Dial,C.F., Faison,K., Melvin,W. and Fecko,C.J. (2012) Quantification of dye-mediated photodamage during single-molecule DNA imaging. *Anal. Biochem.*, **426**, 13–21.
35. Sen,O., Saurin,A.T. and Higgins,J.M.G. (2018) The live cell DNA stain SiR-Hoechst induces DNA damage responses and impairs cell cycle progression. *Sci. Rep.*, **8**, 7898.
36. Bielawski,K., Woczyski,S. and Bielawska,A. (2001) DNA-binding activity and cytotoxicity of the extended diphenylfuran bisamidines in breast cancer MCF-7 cells. *Biol. Pharm. Bull.*, **24**, 704–706.
37. Durand,R.E. and Olive,P.L. (1982) Cytotoxicity, mutagenicity and DNA damage by Hoechst 33342. *J. Histochem. Cytochem.*, **30**, 111–116.
38. Haraguchi,T., Ding,D.Q., Yamamoto,A., Kaneda,T., Koujin,T. and Hiraoka,Y. (1999) Multiple-color fluorescence imaging of chromosomes and microtubules in living cells. In *Cell Struct. Funct.*, **24**, 291–298.
39. Martin,R.M., Leonhardt,H. and Cardoso,M.C. (2005) DNA labeling in living cells. *Cytom. Part A*, **67**, 45–52.
40. Kolb,H.C., Finn,M.G. and Sharpless,K.B. (2001) Click chemistry: diverse chemical function from a few good reactions. *Angew. Chemie Int. Ed.*, **40**, 2004–2021.
41. Zessin,P.J.M., Finan,K. and Heilemann,M. (2012) Super-resolution fluorescence imaging of chromosomal DNA. *J. Struct. Biol.*, **177**, 344–348.
42. Salic,A. and Mitchison,T.J. (2008) A chemical method for fast and sensitive detection of DNA synthesis in vivo. *Proc. Natl. Acad. Sci. U.S.A.*, **105**, 2415–2420.
43. Qu,D., Wang,G., Wang,Z., Zhou,L., Chi,W., Cong,S., Ren,X., Liang,P. and Zhang,B. (2011) 5-Ethynyl-20-deoxycytidine as a new agent for DNA labeling: Detection of proliferating cells. *Anal. Biochem.*, **417**, 112–121.
44. Kotogány,E., Dudits,D., Horváth,G. V. and Ayaydin,F. (2010) A rapid and robust assay for detection of S-phase cell cycle progression in plant cells and tissues by using ethynyl deoxyuridine. *Plant Methods*, **6**, 5.
45. Spahn,C., Endesfelder,U. and Heilemann,M. (2014) Super-resolution imaging of *Escherichia coli* nucleoids reveals highly structured and asymmetric segregation during fast growth. *J. Struct. Biol.*, **185**, 243–249.
46. Spahn,C., Cella-Zannacchi,F., Endesfelder,U. and Heilemann,M. (2015) Correlative super-resolution imaging of RNA polymerase distribution and dynamics, bacterial membrane and chromosomal structure in Escherichia coli. *Methods Appl. Fluoresc.*, **3**, 014005.
47. Ferullo,D.J., Cooper,D.L., Moore,H.R. and Lovett,S.T. (2009) Cell cycle synchronization of *Escherichia coli* using the stringent response, with fluorescence labeling assays for DNA content and replication. *Methods*, **48**, 8–13.
48. Zhao,H., Halicka,H.D., Li,J., Biela,E., Berniak,K., Dobrucki,J. and Darzynkiewicz,Z. (2013) DNA damage signaling, impairment of cell cycle progression, and apoptosis triggered by 5-ethynyl-2′-deoxyuridine incorporated into DNA. *Cytom. Part A*, **83**, 979–988.
49. Ligasová,A., Liboska,R., Friedecký,D., Mičová,K., Adam,T., Ozdian,T., Rosenberg,I. and Koberna,K. (2016) Dr Jekyll and Mr Hyde: A strange case of 5-ethynyl-2′-deoxyuridine and 5-ethynyl-2′-deoxycytidine. *Open Biol.*, **6**, 150172.
50. Kanda,T., Sullivan,K.F. and Wahl,G.M. (1998) Histone-GFP fusion protein enables sensitive analysis of chromosome dynamics in living mammalian cells. *Curr. Biol.*, **8**, 377–385.
51. Kimura,H. and Cook,P.R. (2001) Kinetics of core histones in living human cells: little exchange of H3 and H4 and some rapid exchange of H2B. *J. Cell Biol.*, **153**, 1341–1353.
52. McKinney,S.A., Murphy,C.S., Hazelwood,K.L., Davidson,M.W. and Looger,L.L. (2009) A bright and photostable photoconvertible fluorescent protein. *Nat. Methods*, **6**, 131–133.
53. Köster,R.W. and Fraser,S.E. (2001) Tracing transgene expression in living zebrafish embryos. *Dev. Biol.*, **233**, 329–346.
54. Fraser,S.T., Hadjantonakis,A.K., Sahr,K.E., Willey,S., Kelly,O.G., Jones,E.A.V., Dickinson,M.E. and Baron,M.H. (2005) Using a histone yellow fluorescent protein fusion for tagging and tracking endothelial cells in ES cells and mice. *Genesis*, **42**, 162–171.
55. Das,T., Payer,B., Cayouette,M. and Harris,W.A. (2003) In vivo time-lapse imaging of cell divisions during neurogenesis in the developing zebrafish retina. *Neuron*, **37**, 597–609.
56. Savoian,M.S. and Rieder,C.L. (2002) Mitosis in primary cultures of *Drosophila melanogaster* larval neuroblasts. *J. Cell Sci.*, **115**, 3061–3072.
57. Boisnard-Lorig,C., Colon-Carmona,A., Bauch,M., Hodge,S., Doerner,P., Bancharel,E., Dumas,C., Haseloff,J. and Berger,F. (2001) Dynamic analyses of the expression of the histone::YFP fusion protein in Arabidopsis show that syncytial endosperm is divided in mitotic domains. *Plant Cell*, **13**, 495–509.
58. Hu,Y.S., Zhu,Q., Elkins,K., Tse,K., Li,Y., Fitzpatrick,J.A.J., Verma,I.M. and Cang,H. (2013) Light-sheet Bayesian microscopy enables deepcell super-resolution imaging of heterochromatin in live human embryonic stem cells. *Opt. Nanoscopy*, **2**, 7.
59. Wery,M., Woldringh,C.L. and Rouviere-Yaniv,J. (2001) HU-GFP and DAPI co-localize on the *Escherichia coli* nucleoid. *Biochimie*, **83**, 193–200.
60. Hadizadeh,N., Johnson,R.C. and Marko,J.F. (2016) Facilitated dissociation of a nucleoid protein from the bacterial chromosome. *J. Bacteriol.*, **198**, 1735–1742.

61. Köhler,P. and Marahiel,M.A. (1997) Association of the histone-like protein HBsu with the nucleoid of Bacillus subtilis. *J. Bacteriol.*, **179**, 2060–2064.
62. Smits,W.K. and Grossman,A.D. (2010) The transcriptional regulator Rok binds A+T-rich DNA and is involved in repression of a mobile genetic element in Bacillus subtilis. *PLoS Genet.*, **6**, e1001207.
63. Hadizadeh Yazdi,N., Guet,C.C., Johnson,R.C. and Marko,J.F. (2012) Variation of the folding and dynamics of the *Escherichia coli* chromosome with growth conditions. *Mol. Microbiol.*, **86**, 1318–1333.
64. Fisher,J.K., Bourniquel,A., Witz,G., Weiner,B., Prentiss,M. and Kleckner,N. (2013) Four-dimensional imaging of E. coli nucleoid organization and dynamics in living cells. *Cell*, **153**, 882–895.
65. Kołodziej,M., Trojanowski,D., Bury,K., Hołówka,J., Matysik,W., Kąkolewska,H., Feddersen,H., Giacomelli,G., Konieczny,I., Bramkamp,M. *et al.* (2021) Lsr2, a nucleoid-associated protein influencing mycobacterial cell cycle. *Sci. Rep.*, **11**, 2910.
66. Marbouty,M., Le Gall,A., Cattoni,D.I., Cournac,A., Koh,A., Fiche,J.B., Mozziconacci,J., Murray,H., Koszul,R. and Nollmann,M. (2015) Condensin- and replication-mediated bacterial chromosome folding and origin condensation revealed by Hi-C and super-resolution imaging. *Mol. Cell*, **59**, 588–602.
67. Heo,M., Nord,A.L., Chamousset,D., Van Rijn,E., Beaumont,H.J.E. and Pedaci,F. (2017) Impact of fluorescent protein fusions on the bacterial flagellar motor. *Sci. Rep.*, **7**, 12583.
68. Zhang,F., Moniz,H.A., Walcott,B., Moremen,K.W., Wang,L. and Linhardt,R.J. (2014) Probing the impact of GFP tagging on Robo1-heparin interaction. *Glycoconj. J.*, **31**, 299–307.
69. Swulius,M.T. and Jensen,G.J. (2012) The helical mreb cytoskeleton in *Escherichia coli* MC1000/pLE7 is an artifact of the N-terminal yellow fluorescent protein tag. *J. Bacteriol.*, **194**, 6382–6386.
70. Gibson,D.G., Young,L., Chuang,R.Y., Venter,J.C., Hutchison,C.A. and Smith,H.O. (2009) Enzymatic assembly of DNA molecules up to several hundred kilobases. *Nat. Methods*, **6**, 343–345.
71. Martin-Ramirez,J., Hofman,M., Van Den Biggelaar,M., Hebbel,R.P. and Voorberg,J. (2012) Establishment of outgrowth endothelial cells from peripheral blood. *Nat. Protoc.*, **7**, 1709–1715.
72. Schindelin,J., Arganda-Carreras,I., Frise,E., Kaynig,V., Longair,M., Pietzsch,T., Preibisch,S., Rueden,C., Saalfeld,S., Schmid,B. *et al.* (2012) Fiji: an open-source platform for biological-image analysis. *Nat. Methods*, **9**, 676–682.
73. Panier,S., Ichijima,Y., Fradet-Turcotte,A., Leung,C.C.Y., Kaustov,L., Arrowsmith,C.H. and Durocher,D. (2012) Tandem protein interaction modules organize the ubiquitin-dependent response to DNA double-strand breaks. *Mol. Cell*, **47**, 383–395.
74. Luijsterburg,M.S., Typas,D., Caron,M.-C., Wiegant,W.W., van den Heuvel,D., Boonen,R.A., Couturier,A.M., Mullenders,L.H., Masson,J.-Y. and van Attikum,H. (2017) A PALB2-interacting domain in RNF168 couples homologous recombination to DNA break-induced chromatin ubiquitylation. *Elife*, **6**, e20922.
75. Schneider,C.A., Rasband,W.S. and Eliceiri,K.W. (2012) NIH Image to ImageJ: 25 years of image analysis. *Nat. Methods*, **9**, 671–675.
76. Typas,D., Luijsterburg,M.S., Wiegant,W.W., Diakatou,M., Helfricht,A., Thijssen,P.E., van den Broek,B., Mullenders,L.H. and van Attikum,H. (2015) The de-ubiquitylating enzymes USP26 and USP37 regulate homologous recombination by counteracting RAP80. *Nucleic Acids Res.*, **43**, 6919–6933.
77. Dame,R.T., Noom,M.C. and Wuite,G.J.L. (2006) Bacterial chromatin organization by H-NS protein unravelled using dual DNA manipulation. *Nature*, **444**, 387–390.
78. Qin,L., Erkelens,A.M., Ben Bdira,F. and Dame,R.T. (2019) The architects of bacterial DNA bridges: a structurally and functionally conserved family of proteins. *Open Biol.*, **9**, 190223.
79. Duan,B., Ding,P., Navarre,W.W., Liu,J. and Xia,B. (2021) Xenogeneic silencing and bacterial genome evolution: mechanisms for DNA recognition imply multifaceted roles of xenogeneic silencers. *Mol. Biol. Evol.*, **38**, 4135–4148.
80. Scott,M.S., Boisvert,F.M., McDowall,M.D., Lamond,A.I. and Barton,G.J. (2010) Characterization and prediction of protein nucleolar localization sequences. *Nucleic Acids Res.*, **38**, 7388–7399.
81. Scott,M.S., Troshin,P. V. and Barton,G.J. (2011) NoD: a nucleolar localization sequence detector for eukaryotic and viral proteins. *BMC Bioinformatics*, **12**, 317.
82. Martin,R.M., Ter-Avetisyan,G., Herce,H.D., Ludwig,A.K., Lättig-Tünnemann,G. and Cardoso,M.C. (2015) Principles of protein targeting to the nucleolus. *Nucleus*, **6**, 314–325.
83. Goedhart,J., Von Stetten,D., Noirclerc-Savoye,M., Lelimousin,M., Joosen,L., Hink,M.A., Van Weeren,L., Gadella,T.W.J. and Royant,A. (2012) Structure-guided evolution of cyan fluorescent proteins towards a quantum yield of 93%. *Nat. Commun.*, **3**, 751.
84. Musinova,Y.R., Lisitsyna,O.M., Golyshev,S.A., Tuzhikov,A.I., Polyakov,V.Y. and Sheval,E. V. (2011) Nucleolar localization/retention signal is responsible for transient accumulation of histone H2B in the nucleolus through electrostatic interactions. *Biochim. Biophys. Acta - Mol. Cell Res.*, **1813**, 27–38.
85. Zhang,M., Chang,H., Zhang,Y., Yu,J., Wu,L., Ji,W., Chen,J., Liu,B., Lu,J., Liu,Y. *et al.* (2012) Rational design of true monomeric and bright photoactivatable fluorescent proteins. *Nat. Methods*, **9**, 727–729.
86. Bindels,D.S., Haarbosch,L., Van Weeren,L., Postma,M., Wiese,K.E., Mastop,M., Aumonier,S., Gotthard,G., Royant,A., Hink,M.A. *et al.* (2016) MScarlet: a bright monomeric red fluorescent protein for cellular imaging. *Nat. Methods*, **14**, 53–56.
87. Rogakou,E.P., Pilch,D.R., Orr,A.H., Ivanova,V.S. and Bonner,W.M. (1998) DNA double-stranded breaks induce histone H2AX phosphorylation on serine 139. *J. Biol. Chem.*, **273**, 5858–5868.
88. Stucki,M., Clapperton,J.A., Mohammad,D., Yaffe,M.B., Smerdon,S.J. and Jackson,S.P. (2005) MDC1 directly binds phosphorylated histone H2AX to regulate cellular responses to DNA double-strand breaks. *Cell*, **123**, 1213–1226.
89. Buck,S.B., Bradford,J., Gee,K.R., Agnew,B.J., Clarke,S.T. and Salic,A. (2008) Detection of S-phase cell cycle progression using 5-ethynyl-2′-deoxyuridine incorporation with click chemistry, an alternative to using 5-bromo-2′-deoxyuridine antibodies. *Biotechniques*, **44**, 927–929.
90. Kawakami,K. (2005) Transposon tools and methods in zebrafish. *Dev. Dyn.*, **234**, 244–254.
91. Kawakami,K. (2007) Tol2: a versatile gene transfer vector in vertebrates. *Genome Biol.*, **8**, S7.
92. Adli,M. (2018) The CRISPR tool kit for genome editing and beyond. *Nat. Commun.*, **9**, 1911.
93. Guzman,L.M., Belin,D., Carson,M.J. and Beckwith,J. (1995) Tight regulation, modulation, and high-level expression by vectors containing the arabinose P(BAD) promoter. *J. Bacteriol.*, **177**, 4121–4130.
94. Takaki,K., Davis,J.M., Winglee,K. and Ramakrishnan,L. (2013) Evaluation of the pathogenesis and treatment of Mycobacterium marinum infection in zebrafish. *Nat. Protoc.*, **8**, 1114–1124.
95. Lau,I.F., Filipe,S.R., Søballe,B., Økstad,O.A., Barre,F.X. and Sherratt,D.J. (2003) Spatial and temporal organization of replicating Escherichia coli chromosomes. *Mol. Microbiol.*, **49**, 731–743.
96. Chertkova,A.O., Mastop,M., Postma,M., van Bommel,N., van der Niet,S., Batenburg,K.L., Joosen,L., Gadella,T.W.J., Okada,Y. and Goedhart,J. (2020) Robust and bright genetically encoded fluorescent markers for highlighting structures and compartments in mammalian cells. bioRxiv doi: https://doi.org/10.1101/160374, 06 July 2017, preprint: not peer reviewed.